MASTER THESIS

IR-Absorption Measurements for Discrimination of Mammalian Cells

Submitted at the Faculty of Electrical Engineering, Vienna University of Technology
in partial fulfilment of the requirements for the degree of
Master of Sciences (Diplomingenieur)

under supervision of

Univ.Prof. Dr. Michael J. Vellekoop
Dipl.-Ing. Sander van den Driesche

by

Christoph Haiden
Matr.Nr. 0525518
Kirchengasse 141, 2732 Würflach

November, 2010

_____

Abstract

In recent years, cancer has been one of the major causes of death. Undoubtedly, the detection and identification of possibly malignant cells in early stages is vital.

Infrared (IR) spectroscopy which is based on the absorption of IR light due to molecular vibrations has proven to be able to distinguish mammalian tumour cells from healthy cells. But instead of recording the whole spectrum with a commercial IR spectrometer a distinction can also be achieved by comparing the absorbance of cell samples at only a few specific wavelengths that are characteristic for certain molecules in the cell membrane.

In this thesis the design and operation of a cost-effective sensor system for IR absorbance measurements at six wavelengths in the 3.3 - 3.7 µm range is described. The sensor setup consists of IR-LEDs (light emitting diodes), a photodiode detector, and optical components such as narrow bandpass filters, mirrors and lenses. CH_2 and CH_3 of acyl chains in the cell membrane show distinct absorbance peaks at specific wavelengths (symmetric and antisymmetric stretch vibrations). Cell membrane alterations associated with tumour formation result in an absorbance change in the CH_2-stretch ratio that can be detected with the sensor system and used for cell type discrimination.

IR absorbance measurements were performed on epithelial kidney cell lines (normal MDCK (Madine Darby Canine Kidney) and malignant Caki-1) and melanoma cell lines (M14, A375, and 518A2). Cell samples were measured dried and suspended in PBS (phosphate buffered saline). Hence, a microfluidic chip made of IR transparent calciumflouride comprising a microchamber for cell suspension liquid was developed and realised. Chip design and fabrication steps are presented in this thesis.

Measurement results show that a clear and reproducible discrimination between healthy and malignant epithelial kidney cells as well as between the three different melanoma cell lines can be achieved by comparing the CH_2- and CH_3-stretches.

Kurzfassung

Dass Krebs in den letzten Jahren eine der häufigsten Todesursachen darstellte, lässt der Detektion und Identifikation möglicher Krebszellen in frühen Stadien zweifellos große Bedeutung zukommen.

Es hat sich gezeigt, dass Infrarotspektroskopie, basierend auf der Absorption von Infrarot-Licht aufgrund molekularer Schwingungen, eine Unterscheidung von Tumor- und gesunden Zellen ermöglicht. Anstatt jedoch das komplette Spektrum von Zellproben mit einem kommerziellen IR-Spektrometer aufzunehmen, kann man die Absorption an bestimmten Wellenlängen vergleichen, welche charakteristisch für spezifische Moleküle in den Zellmembranen sind.

In dieser Arbeit wird der Entwurf und Betrieb eines Sensorsystems für Infrarot-Absorptionsmessungen an sechs Wellenlängen im Bereich 3.3 - 3.7 µm beschrieben. Der Aufbau besteht aus IR-LEDs, einer Photodiode als Detektor und optischen Komponenten, wie etwa Filter, Spiegel und Linsen. Die symmetrischen und antisymmetrischen Streckschwingungen der CH_2 und CH_3 Moleküle der Acylketten zeigen ausgeprägte Absorptionsmaxima bei bestimmten Wellenlängen. Veränderungen in der Zellmembran aufgrund von Tumorbildung führen zu einer Änderung der Absorption, welche mit dem Sensorsystem aufgezeichnet und zur Unterscheidung von Zelltypen herangezogen werden kann.

Infrarot-Absorptionsmessungen wurden an Nierenepithelzellen (normalen MDCK (Madine Darby Canine Kidney) und bösartigen Caki-1-Zellen) sowie drei Melanomzelllinien (M14, A375 und 518A2) durchgeführt. Zellproben wurden sowohl getrocknet als auch suspendiert in PBS (phosphatgebufferte Salzlösung) gemessen. Aus diesem Grund wurde auch ein Mikrofluidik-Chip aus infrarot-transparentem Calziumflourid mit einer Mikrokammer für Zellsuspension enwickelt und hergestellt. Das Design und die Fabrikation des Chips werden in dieser Arbeit vorgestellt.

Die Messergebnisse zeigten, dass anhand eines Vergleiches der CH_2- und CH_3-Streckschwingungen eine deutliche und reproduzierbare Unterscheidung zwischen gesunden und bösartigen Nierenepithelzellen sowie zwischen den Melanomzelllinien erzielt werden kann.

Acknowledgements

This project is a part of the EU Marie Curie Research Training Network (MRTN) "On-Chip Cell Handling and Analysis" CellCheck. Project no. MRTN-CT-2006-035854.

First and foremost, I would like to thank Univ.Prof. Dr.techn. Michael J. Vellekoop, the head of the Institute of Sensor and Actuator Systems, for the opportunity to work in such an interesting field of research and for writing my thesis under his supervision. Secondly, but not less important, I am grateful to Dipl.-Ing. Sander van den Driesche for all his support, encouragement and advices in technical and non-technical matters throughout my work.

Thanks go to Priv.-Doz. Dr. Christine Hafner and Nina Balazs (Center of Pathophysiology, Infectiology & Immunology, Medical University of Vienna, Vienna, Austria) and Wojciech Witarski, M.Sc., (Institute of Virology, Slovak Academy of Sciences, Bratislava, Slovakia) for readily supplying us with cell samples.

Also, I would like to thank Ing. Edeltraud Svasek and Ing. Peter Svasek for the fabrication of the devices and their helpful comments as well as all the other colleagues at the institute for the constructive conversations and pleasant working atmosphere.

Last but not least, I am particularly thankful for all the support provided by my family and friends throughout those years of studying. Without their help and appreciation I would not have been able to pursue my way and achieve what I have achieved so far - justifiably, they deserve my deepest gratitude.

Table of Contents

Nomenclature

ATR	attenuated total reflectance
AZ4512	negative photoresist
AZ826MIF	photoresist developer
CaF_2	calciumflouride
DAQ	data acquisition
DNA	deoxyribonucleic acid
DMEM	Dulbecco's Modified Eagle Medium
ECM	extracellular matrix
FCS	Fetal Calf Serum
FTIR	Fourier Transform IR
FWHM	full width at half maximum
GBL	gammabutyrolactone
H&E	haemotoxylin and eosin
IR	infrared
$K_2S_2O_8$	potassium peroxydisulfate
KOH	potassium hydroxide
LED	light emitting diode
M	molar
MDCK	Madine Darby Canine Kidney
MEMS	microelectromechanical system
NaOH	sodium hydroxide
NBP	narrow band-pass filter
PBS	phosphate buffered saline
PD	photodiode
PDMS	poly-dimethyl-siloxane
PEB	post-exposure-bake
PGMEA	propylene glycol monomethyl-ether-acetate

QCL	quantum cascade laser
RNA	ribonucleic acid
RPMI	Roswell Park Memorial Institute medium
SB	soft-bake
SU-8	epoxy based negative photoresist
UV	ultraviolet

A	absorbance [-]
C	concentration [mol/liter]
E^{λ}	molar extinction coefficient (molar absorptivity) [$M^{-1}cm^{-1}$]
I	intensity [W/m^2]
T	transmittance [-]
α	absorptance [-]
λ	optical wavelength [µm]

1 Introduction

According to a report of the World Health Organization in 2004 cancer accounted for 7.4 million fatalities worldwide, that is 13 % of all deaths. Hence, it is the leading cause of death, with especially lung, stomach, liver, colon and breast cancer contributing to it. Fatalities due to cancer are projected to continue rising, with an estimated 12 million in 2030 [1]. Moreover, patients with advanced melanoma or kidney cancer show a very low five-year survival rate [2]. Unsurprisingly, the development of diagnostic tools for tumour screening, detection and identification of possible malignant cells plays an important role in understanding tumour development and selecting proper treatment.

The initiation and progression of tumour development is a multifactorial process, that emerges from genetic and molecular defects and also influences cell-cell/cell-extracellular matrix (ECM) interactions [3, 4]. A tumour is a solid neoplasm, i.e. mass of tissue due to abnormal cell proliferation, and it can be benign, pre-malignant or malignant. A malignant tumour originates from the transformation of normal cells into carcinoma cells which become unresponsive to normal physiological controls regulating cell proliferation and apoptosis, i.e. programmed cell death, thus exhibiting a much higher rate of proliferation than cell death or simply uncontrolled growth.

Another form of apoptosis, aniokis, is induced in normal cells upon losing adhesion to the ECM in order to prevent cells from being in the wrong location [5]. While benign or pre-malignant cancers do not spread from the initial tumour site, invasive and metastatic cells, however, do have the ability to migrate from the original tumour and invade surrounding tissues or circulate through blood/lymphatic system. This process will facilitate the formation of secondary tumours in other, often distant organs. As a consequence of tumour growth the organism will eventually suffer from local or systemic implications, such as vital organ dysfunction or uncontrollable infections [3, 6, 7]. Also, metastatic melanoma shows a very high resistance to anti-cancer medication which complicates the patient's chemotherapy or even renders it impossible [8].

Understandably, detection of cancer in early stages, e.g. pre-malignant, that means before it advances or even metastatizes, is the most important factor in increasing the overall survival rate of cancer patients.

Current tumour screening highly relies on the interpretation of histopathologists. The usual procedure includes removal of suspicious tissue samples (biopsies) followed by fixation, that is preservation of the tissue from decay. In order to reveal cellular components like nuclei and cytoplasm, staining is done, e.g. with haemotoxylin and eosin (H&E) [9]. Finally, several pathologists

examine the processed sample with a microscope and interpret the results. Forementioned steps are often expensive, time-consuming, and have to be performed by highly trained personnel. Since histopathology is somewhat subjective, it is associated with inter-observer disagreement as well as false positives and negatives [10, 11].

Infrared (IR) spectroscopy, the absorption of infrared light due to specific molecular vibrations, allows for rapid analysis of biological tissue and cell components such as lipids, proteins, RNA or DNA without the need of labelling or staining. It is capable of providing a more objective diagnostic assessment compared to histopathology. Biochemical changes due to cancer development can be observed from the spectral data and potentially enable the detection of molecular changes that precede morphological changes, hence facilitating an earlier diagnosis of dysplasia [12].

In the past two decades IR absorbance spectra of several types of normal and cancer cells have been recorded and published in literature. A comparison of those spectra led to the introduction of a set of spectral differences or biomarkers. The results suggest that a clear differentiation between healthy and malignant cells by means of IR absorbance comparison is feasible. Furthermore, instead of measuring the whole spectrum comparing the absorbance at only a few characteristic wavelengths could reduce the complexity of the IR spectroscopy system. On that account *Driesche et al.* recently proposed a four wavelength sensor system for label-free cell analysis by means of measuring the CH_2-symmetric / CH_2-antisymmetric stretch ratio of mammalian cells [13, 14, 15, 16].

In this thesis the further development of the four wavelength sensor system is described. This includes the implementation of two additional wavelengths for the CH_3-stretches and the development of a microfluidic chip in order to measure live cells in suspension. Experiments with dried cells and cells suspended in phosphate buffered saline (PBS) were conducted and the results are discussed.

The next chapter comprises fundamentals of IR spectroscopy and cell structures and provides a brief overview of promising publications dealing with IR absorbance studies on cancer cells. In chapter three the previously introduced sensor system and modifications in the course of this thesis are specified. Experiments with dried cells are described in chapter four. Theoretical considerations on the development of a microfluidic chip as well as the design steps and fabrication are provided in chapter five. Suspended cell measurements that were conducted with this chip are described in chapter six. Finally, conclusions and an outlook are presented in chapter seven.

2 Theory

In this chapter an overview about IR spectroscopy as a discrimination tool will be given. Also basics about the cell membrane structure will be explained. Moreover, the findings from literature research concerning spectral differences between normal and cancer cells will be discussed.

2.1 IR spectroscopy

Infrared spectroscopy is based on the absorption of infrared radiation (spectral range: 740 nm to 1000 µm, see Fig. 2.1) by matter due to the vibrational modes of chemical bonds. A molecular vibration is the periodic motion of atoms in a molecule with a certain frequency. If molecules absorb electromagnetic radiation at specific resonance frequencies, being characteristic for their structure, then vibrations are excited and accordingly more IR radiation is absorbed. Depending on its number of atoms, a molecule can vibrate in several ways, called vibrational modes. For example the H_2O molecule has symmetric and antisymmetric stretch modes, bending or scissoring, wagging, twisting and rocking (see Fig. 2.2) [17].

When infrared light is focused on a sample then a fraction of the incident light is absorbed while another fraction is passed through. The absorption varies with the wavelength and absorption bands specific to the chemical compounds present in the sample are formed. The output of an IR spectrometer consists of the recorded transmittance or absorbance of the sample over the wavelength and is referred to as a spectrum. Fig. 2.3 shows an exemplary spectrum with the ordinate scale presented by the absorbance. The relation between absorbance and transmittance is described in Eq. 2.1.

$$A = -log(T) = -log(\frac{I}{I_0}), \tag{2.1}$$

A is the absorbance, T is the transmittance and I and I_0 are the intensities of the transmitted and incident light, respectively. Absorbance must not be mistaken with the term absorbtance or absorbtion factor (α) which describes the ratio of absorbed to incident radiation power and is therefore $\alpha = 100\,\%$ - T (in %) [18]. Instead of the wavelength in [µm] it is also common, especially amongst chemists, to use the wavenumber in inverse centimeters [cm^{-1}] which is simply the reciprocal of the wavelength.

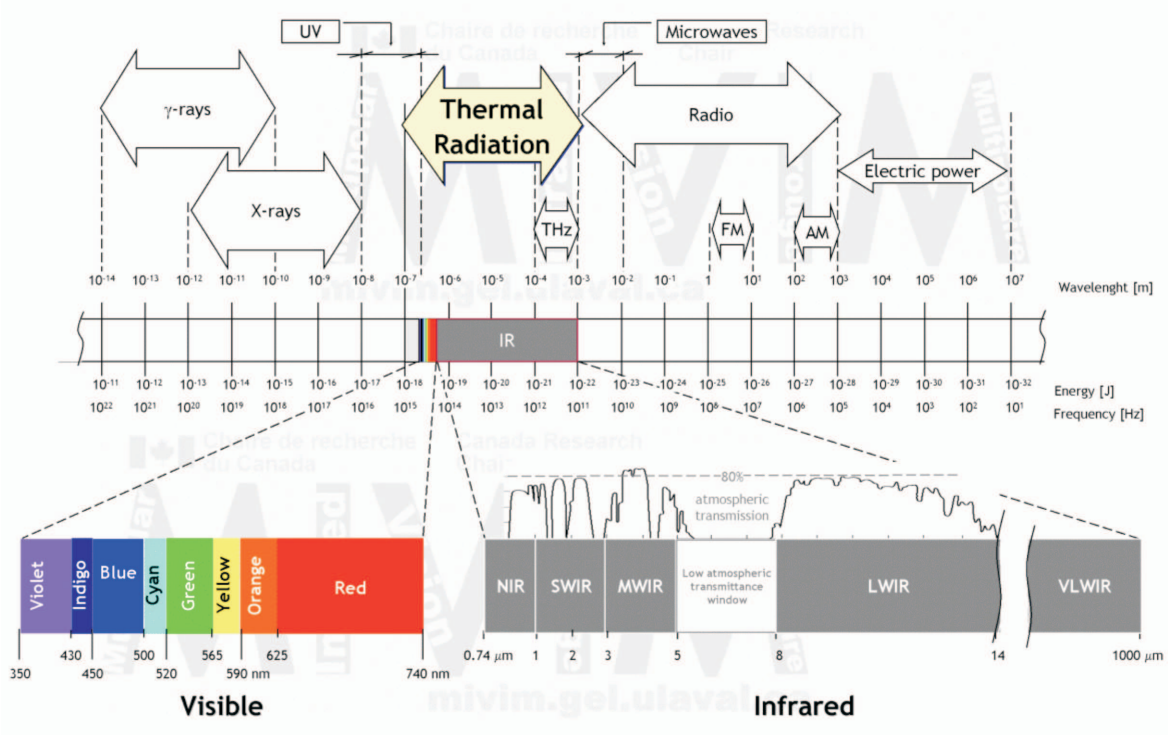

Figure 2.1: Electromagnetic spectrum, IR ranges from 740 nm to 1000 µm [19].

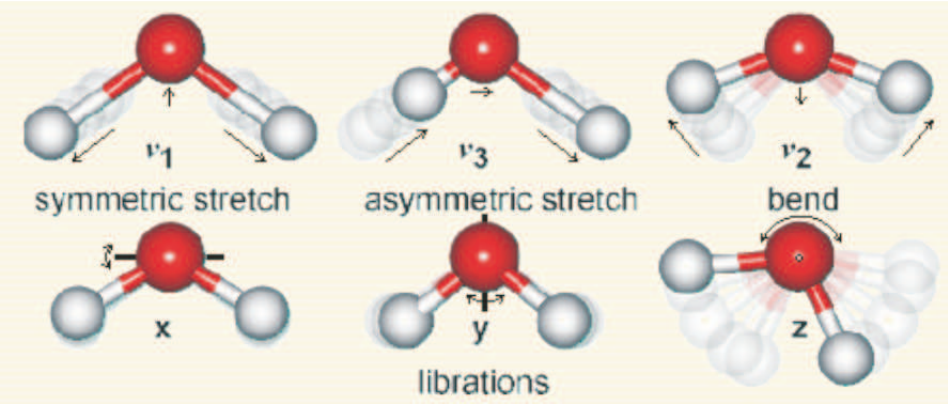

Figure 2.2: Vibrational modes of water: symmetric and antisymmetric stretch, bending, as well as librations in direction of the x-, y-, and z-axis (wagging, twisting, and rocking) [20].

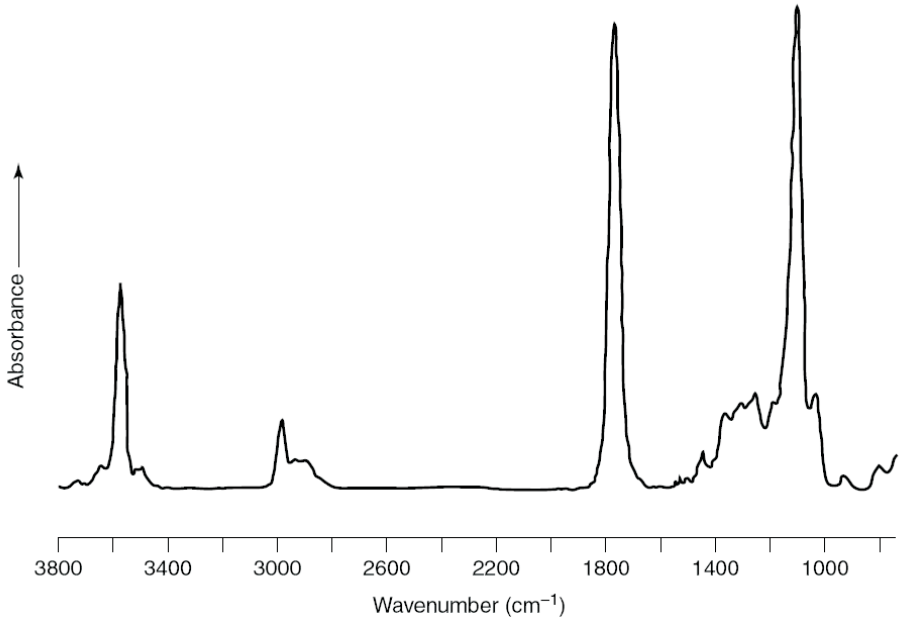

Figure 2.3: Absorbance spectrum of lactic acid [17].

Currently, the most common technique is called FTIR (Fourier Transform IR) spectroscopy, which utilizes computer processing in order to convert raw data from interferograms into an actual spectrum by means of Fourier transformation. FTIR is often combined with attenuated total reflectance (ATR) which makes use of the phenomenon of total internal reflection. If a beam enters a crystal in such a way that it undergoes internal reflection then it penetrates a fraction of a wavelength beyond the reflecting surface. A sample brought in close contact to this surface causes the beam to lose energy at the material specific absorption wavelengths and the resulting attenuated radiation can be measured. A detailed description of the structure and working principle of ATR-FTIR devices can be found in [17].

2.2 IR spectroscopy of cell membranes

IR spectroscopy is an interesting tool that can be used for the identification of organic compounds like hydrocarbons and the study of biological molecules without the need of additional labels. Various biological systems like lipids, proteins, peptides and biomembranes have been studied using IR spectroscopy [17, 21].

Mammalian cells are enclosed by a cell membrane which acts as a boundary between the extracellular environment and the cytoplasm, the inside of the cell. Membranes consist mostly of lipid molecules arranged in a double layer, the lipid bilayer (see Fig. 2.4) and proteins, e.g. receptors or proteins which transport specific molecules across the membrane. The most abundant type of membrane lipids are phospholipids (see Fig. 2.5), which consist of a polar head group and two uncharged hydrophobic hydrocarbon tails, called fatty acids. In case of saturated fatty acids these

acyl chains are basically chains of methylen (CH_2) groups with a terminal methyl (CH_3) molecule. Unsaturated fatty acids contain at least one double bond (see Fig. 2.6). Phosphatidylcholine for instance consists of one saturated and one unsaturated fatty acid and the polar head group is a choline molecule [22].

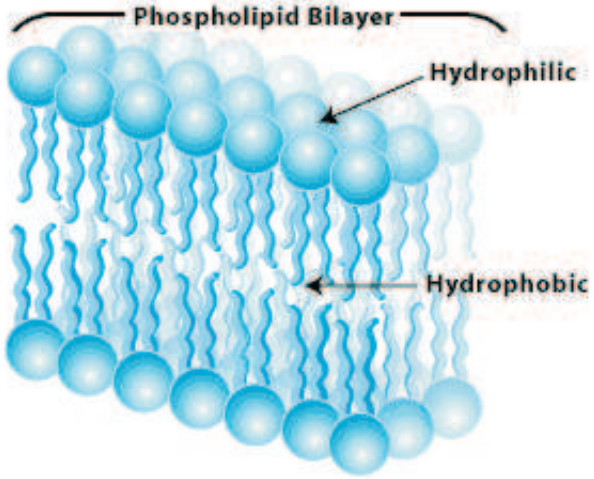

Figure 2.4: Schematic of a lipid bilayer [23].

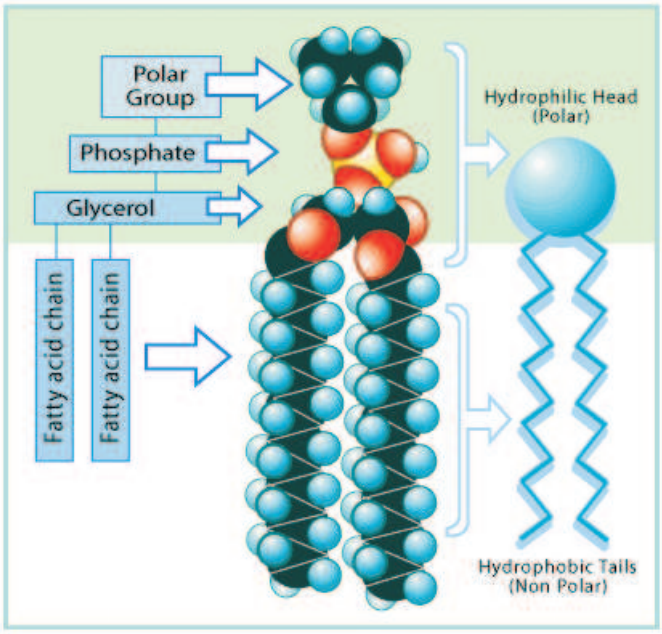

Figure 2.5: Schematic of a phospholipid [23].

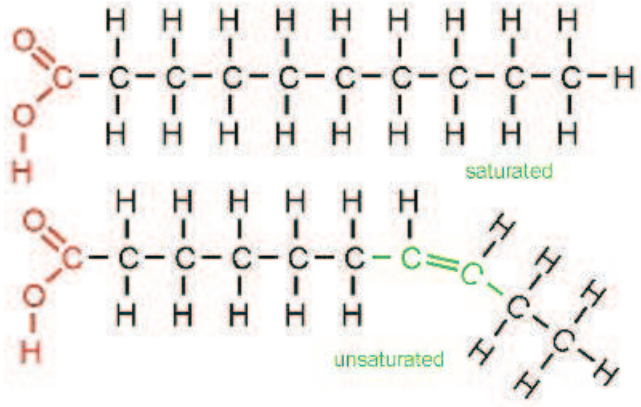

Figure 2.6: Examples for saturated and unsaturated fatty acids [24].

IR spectroscopy is now able to provide valuable information about lipid structure in membranes. For instance, the most intense lipid vibrations in the 2800 - 3000 cm^{-1} region are that of the CH_2 symmetric and antisymmetric stretch. Tab. 2.1 shows the absorption bands of CH_2 and CH_3.

Table 2.1: Wavenumber and corresponding wavelength of the CH_2 and CH_3 stretch absorption bands. Data according to [17, 21].

CH stretching mode	Wavenumber [cm^{-1}]	Wavelength [µm]
CH_3 antisymmetric ($\nu_{as}CH_3$)	2956	3.383
CH_2 antisymmetric ($\nu_{as}CH_2$)	2920	3.425
CH_3 symmetric ($\nu_{s}CH_3$)	2870	3.484
CH_2 symmetric ($\nu_{s}CH_2$)	2850	3.509

2.3 Absorption spectra of cancer cells

Several research groups studied normal and malignant tissue samples by means of IR spectroscopy, especially in the mid-IR range (400 - 4000 cm^{-1}), and found significant differences at characteristic wavelengths. Fig. 2.7 shows a schematic diagram of the absorbance spectrum of mammalian cells in the 2800 - 3000 cm^{-1} region. The absorbance values at the outer left and right of the spectrum are used for baseline correction in order to obtain the functional absorbance values at the CH_2 and CH_3 absorbtion peaks. In turn, these baseline corrected values can be used to compare different cell samples.

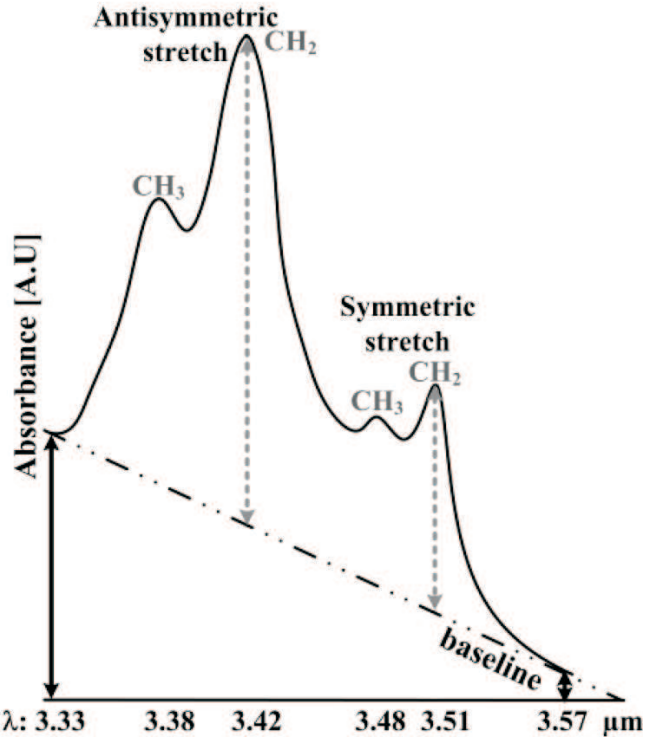

Figure 2.7: Absorbance spectrum example of mammalian cells in the 2800 - 3000 cm^{-1} region (3.33 µm - 3.57 µm) [14].

With regard to the developed and realized sensor system ([13]) the results from those publication dealing with changes in the CH_2 and CH_3 absorption bands shall now be summarized:

Rigas et al. studied tissue sections of human colorectal cancer and histologically normal mucosa 5 - 10 cm away from the tumour by means of FTIR. A comparison of the spectra is depicted in Fig. 2.8. In malignant tissue the $\nu_s CH_2$ mode at 2850 cm^{-1} was increased, while $\nu_s CH_3$ and $\nu_{as} CH_3$ were decreased compared to $\nu_{as} CH_2$ at 2920 cm^{-1} [25]. The $\nu_{as} CH_2$ mode has the highest absorbance and is therefore commonly used for normalization of the spectra.

Maziak et al. found that in malignant esophageal tissue $\nu_s CH_2$ was increased, while $\nu_s CH_3$ and $\nu_{as} CH_3$ were decreased (Fig. 2.9) [26].

Anastassopoulou et al. compared pathological breast tissue with connective tissue (Fig. 2.10) and found the $\nu_s CH_2$ to be increased, while $\nu_s CH_3$ and $\nu_{as} CH_3$ were decreased [27].

Fabian et al. also compared benign and malignant breast tissue (Fig. 2.11), $\nu_s CH_2$ was increased, $\nu_s CH_3$ and $\nu_{as} CH_3$ were decreased [28]. As demonstrated in Fig. 2.7 above, a simple baseline correction by scaling and rotating was applied in order to be able to compare the benign fibroadenoma spectrum with the malignant tissue spectrum.

Driesche et al. measured the IR absorbance of epithelial kidney cells, namely healthy MDCK (Madin Darby Canine Kidney) and carcinoma Caki-1 [13]. They found all $\nu_s CH_2$, $\nu_s CH_3$ and $\nu_{as} CH_3$ to be increased (Fig. 2.12).

Zwielly et al. conducted experiments with cisplatin-resistant and non-resistant melanoma cell lines, GAC and GA, respectively. Cisplatin is a common anti-cancer drug that triggers apoptosis

in cells by crosslinking their DNA. However, if drug resistance occurs in cancer cells chemotherapy becomes ineffective [8]. In resistant cells $\nu_s CH_2$ was increased while $\nu_s CH_3$ and $\nu_{as} CH_3$ were decreased with respect to $\nu_{as} CH_2$ (Fig. 2.13). If cisplatin-resistant cells are interpreted as a more severe type of cancer, which seems reasonable, then those findings are in accord with the aforementioned ones.

Concordantly, the results from the above publications state that the $\nu_s CH_2$ absorbtion peak is higher in tumour cells than in normal cells.

Even though it is still unclear what the molecular mechanism is that leads to a change in $\nu_s CH_2$ and $\nu_{as} CH_2$ of mammalian plasma membranes it is clear that during tumour formation the cell membrane changes. In breast tumour cells for example a cell membrane located growth factor encoded by HER-2 genes is over-expressed [29]. Also changes in the composition of integrin, a membrane molecule that is responsible for cell-cell adhesion and therefore involved in metastasis progression, are presented [30, 31].

At any rate, previously listed findings indicate that the $\nu_s CH_2/\nu_{as} CH_2$ stretch ratio would be useful in order to distinguish healthy and malignant cells as it was performed in [13, 14, 15, 16]. Also, an investigation of the $\nu_s CH_3$ and $\nu_{as} CH_3$ absorbance stretches is suggested.

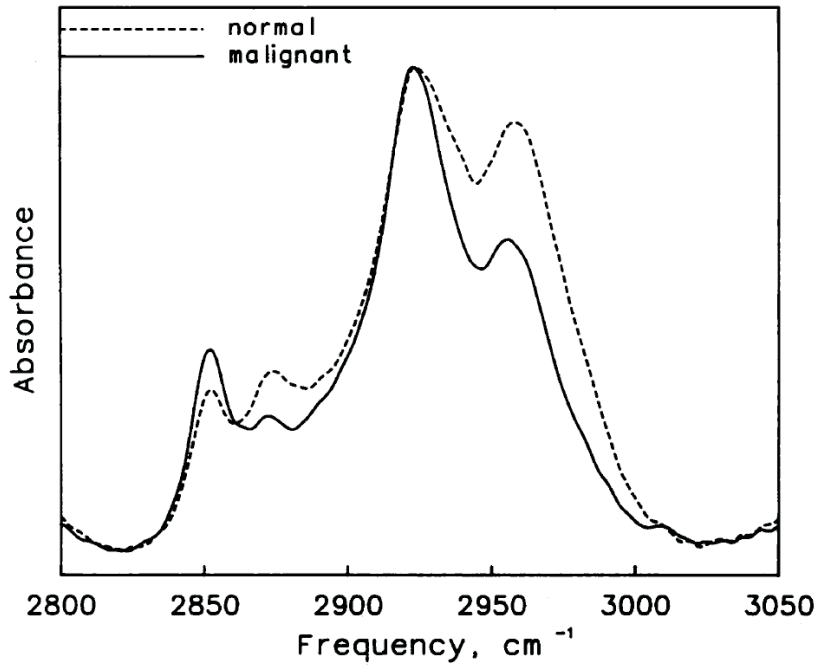

Figure 2.8: IR spectra of normal and malignant colon tissues, both spectra are normalized on the $\nu_{as} CH_2$ peak [25].

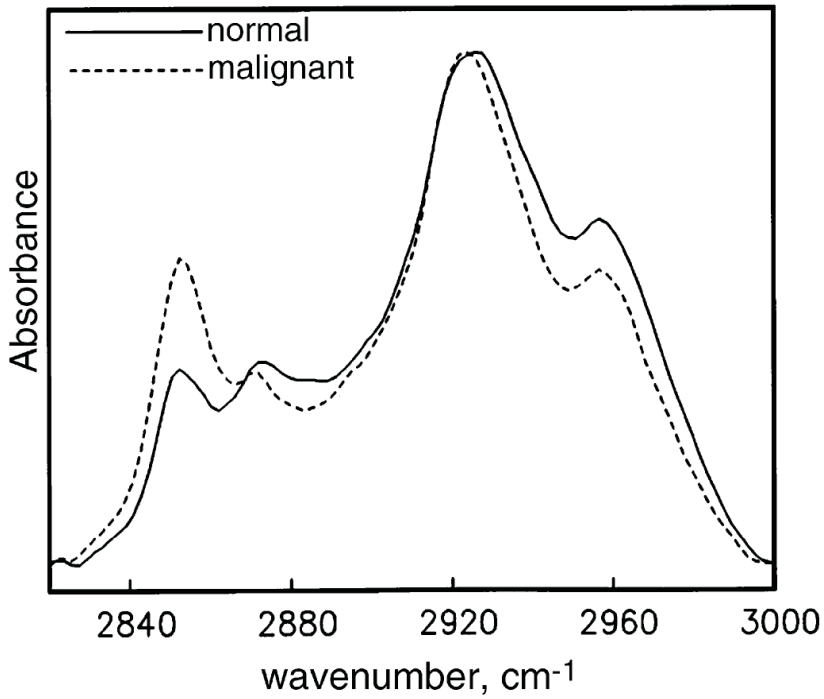

Figure 2.9: IR spectra of normal and malignant esophageal tissues [26].

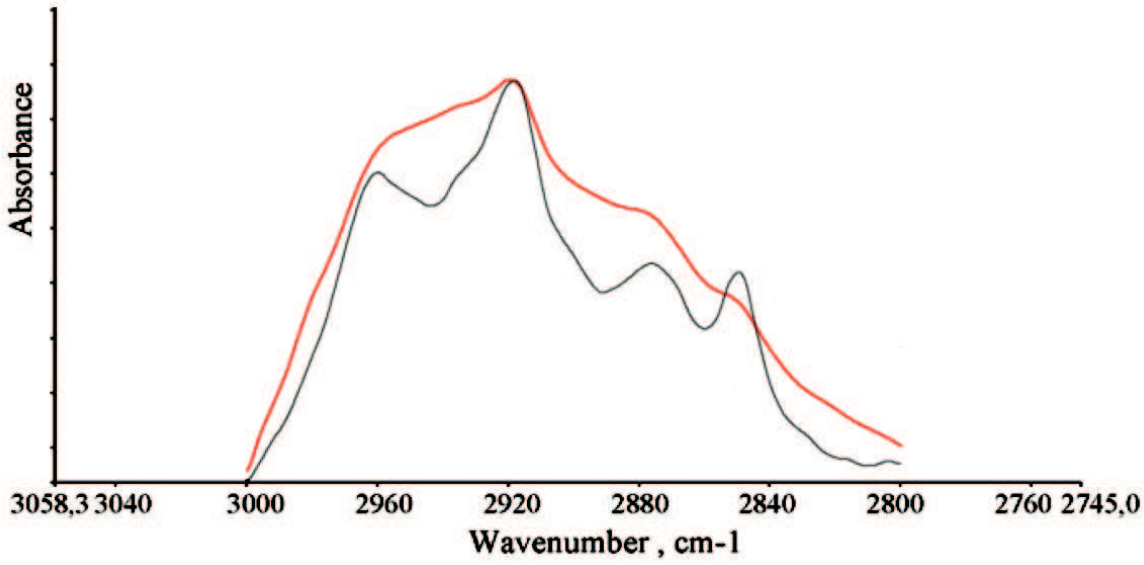

Figure 2.10: IR spectra of cancerous (black) and connective (red) breast tissues. Figure adapted from [27].

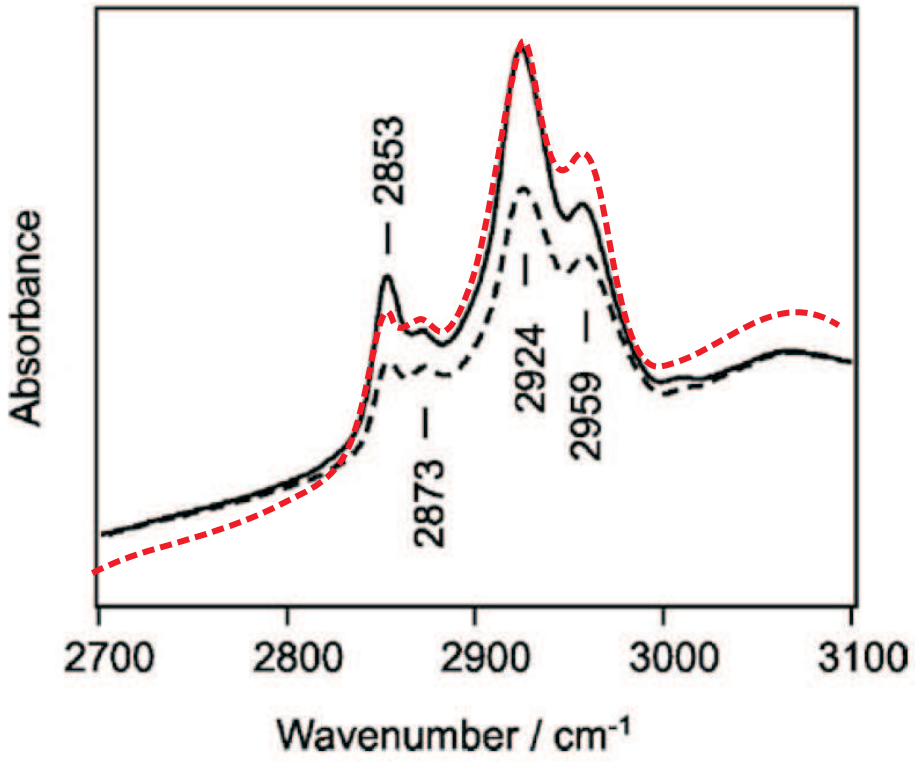

Figure 2.11: IR spectra of benign and malignant breast tissues. Figure adapted from [28]. The solid line depicts invasive ductal carcinoma, the dashed line represents the epithelium of a fibroadenoma, a benign lesion. For better visibility of the CH-peaks, the fibroadenoma line was enlarged and rotated (red, dotted line).

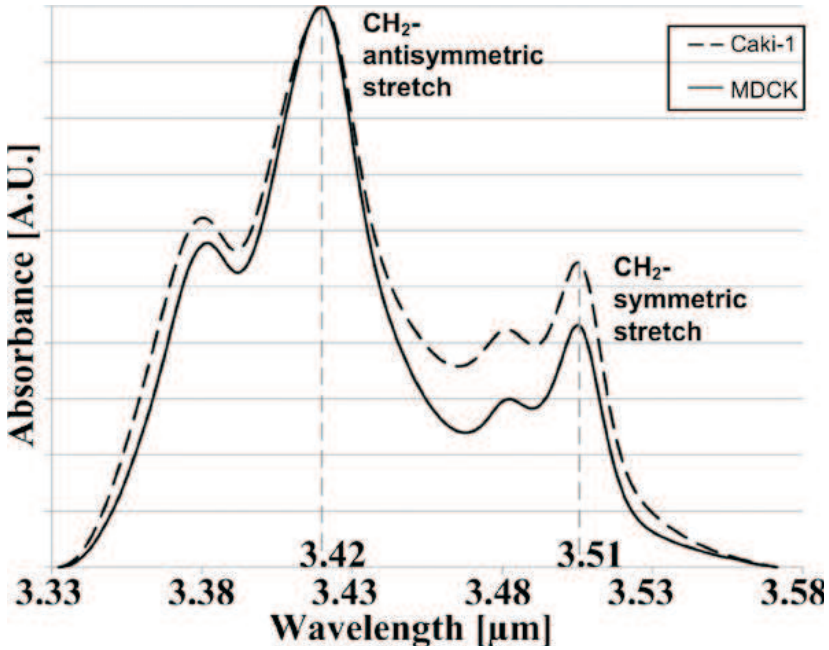

Figure 2.12: IR spectra of healthy (solid line) and carcinoma (dashed line) epithelial kidney cells [13].

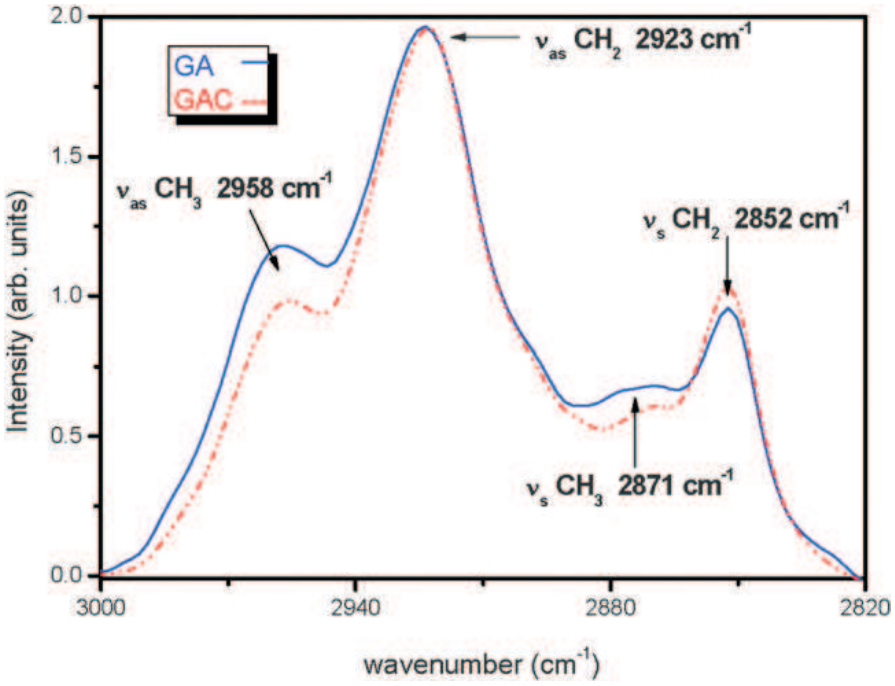

Figure 2.13: IR spectra of cisplatin-resistant (red, dashed line) and non-resistant (blue, solid line) melanoma cells [8].

3 Sensor System

In this chapter the basic concept of the quadruple wavelength sensor system (presented in [13, 14, 15, 16]) and its specifications are summarized. Several hardware modifications have been carried out during this thesis work. Finally, the data acquisition and calculation steps, in order to obtain comparable measurement values from the cell sample measurements, will be explained.

3.1 The quadruple wavelength sensor system

As mentioned in the previous chapter, the cell type discrimination concept is based on differences of cell specific absorption bands in the wavelength range between 3.3 - 3.7 µm (lipid CH_2 and CH_3 stretches). While it is possible to record the entire IR absorbance spectrum between 2 - 20 µm with a commercial FTIR spectrometer (see Fig. 3.1) they are rather bulky and expensive laboratory devices, often requiring liquid nitrogen cooled infrared detectors. The measurement of only a few specific wavelengths, however, does not afford such complex equipment. Instead, a cost-effective system comprising a photodiode and light emitting diodes (LED) suitable for the 3.0 - 3.7 µm range can be used. A block diagram and a photograph of the sensor system can be found in Fig. 3.2.

By measuring and comparing a ratio, samples of different thickness can be compared. Furthermore, a baseline correction is required to compensate for e.g. the water fraction present in the cells of interest. Hence, it is not only necessary to measure the functional absorbance bands but also two base points, namely 3.33 - 3.57 µm, that describe the baseline of the signal (compare Fig. 3.3). The procedures to obtain baseline corrected absorbance values and subsequently calculate normalized absorbance ratios are explained in section 3.4.

Figure 3.1: Example of a commercial FTIR spectrometer used in analytical chemistry (Bruker Equinox 55) [32]. Spectral range is 400 - 12000 cm^{-1} (0.83 - 25 µm), spectral resolution is 0.20 cm^{-1} [33].

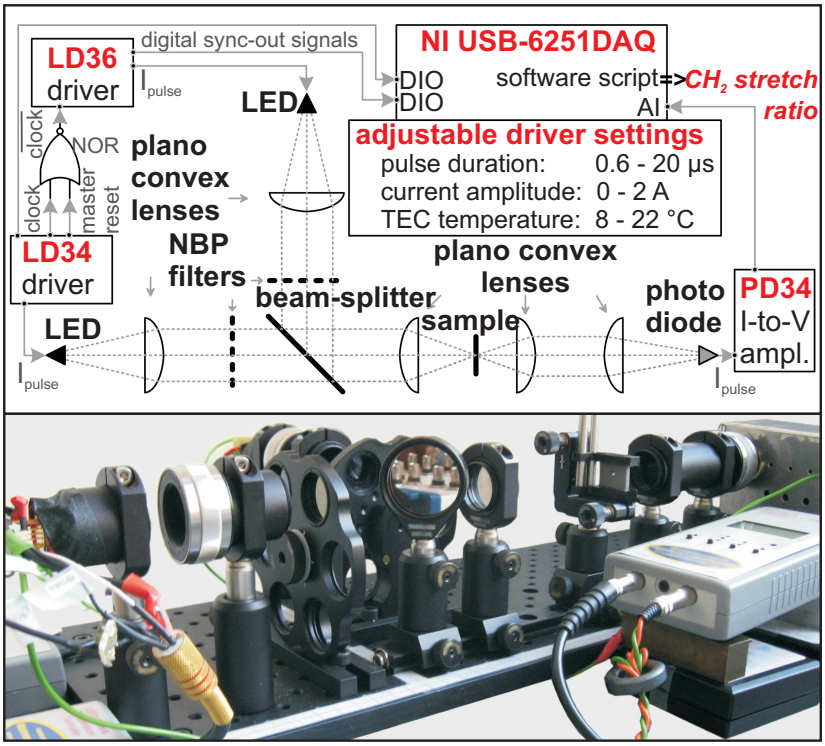

Figure 3.2: (Top) Block diagram of the sensor system comprising electronic and optical components (LEDs, drivers, photodiode, amplifier, data acquisition board; collimation lenses, filters, beam splitter). (Bottom) Photograph of the sensor setup [13].

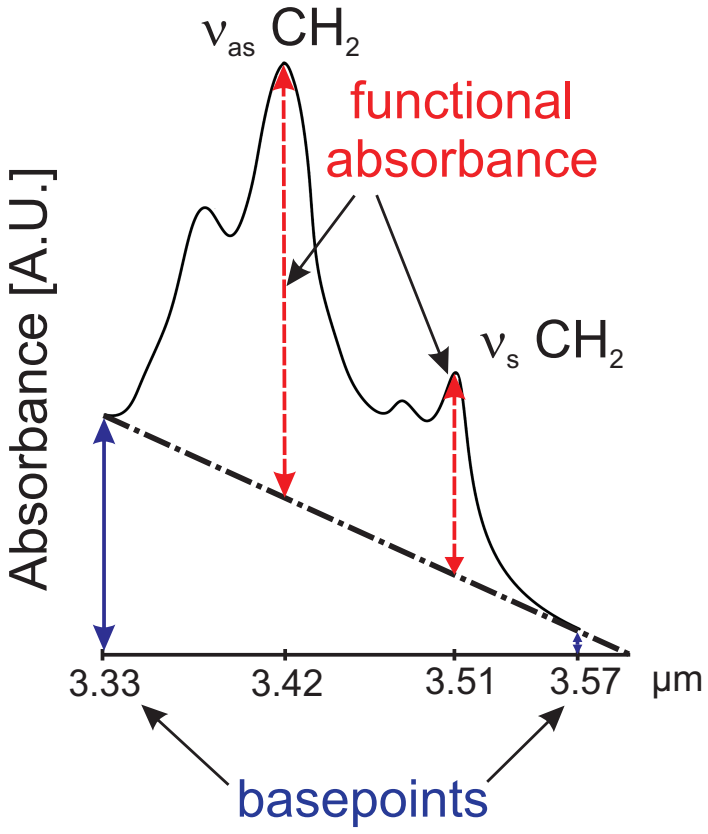

Figure 3.3: The functional absorbance of a sample is the fraction of the total absorbance above the baseline. In order to calculate the functional absorbance, the baseline influence has to be eliminated (baseline correction).

To cover the IR region between 3.33 and 3.57 µm two LEDs with centre wavelengths at 3.4 and 3.6 µm are used as infrared light sources, while the detector is a photodiode with a centre wavelength of 3.35 µm (see diode specifications in Tab. 3.1). The LEDs are emitting 10 µs pulses alternately with a frequency of 2 kHz (see Fig. 3.4). The light from each LED is collimated by plano-convex lenses and directed at a filter wheel with changeable narrow band pass filters. Those filters can be manually changed and as a result only specific wavelengths from each LED can be selected. That is, 3.33 µm (first base-point) and 3.425 µm (CH_2 - antisymmetric) for LED34 as well as 3.57 µm (second base-point) and 3.51 µm (CH_2 - symmetric) for LED36.

After passing the filters the pulsed light beams are combined by means of a beam splitter. A plano-convex lens focusses the beams through a 1.5 mm aperture on the sample that is fixed perpendicular to the light beam on a horizontal sample holder. The light passing through the sample is further directed to the photodiode. The photodiode output signal is current-to-voltage amplified and recorded only when a LED is emitting. This is achieved by connecting the digital synchronisation signal of both LED drivers and the analogue photodiode signal to a data acquisition board (NI USB-6251DAQ) operated with a MATLAB script. By means of this method the absorbance values at two wavelengths can be measured simultaneously. During operation the photodiode signal is also observed with an oscilloscope. This way it is possible to make the IR pulses visible and to see if the sample thickness is adequate for the measurements. Detailed data

acquisition steps and further processing of the recorded signal will be described in sections 3.3 and 3.4.

Table 3.1: LED and photodiode specifications at 22°C. Data according to [13].

	LED34	LED36	Photodiode	
Peak wavelength	3.4 ± 0.05	3.65 ± 0.05	3.35	[µm]
Pulsed power @ I=1A	500 ± 100	350 ± 70	-	[µW]
Switching time	≤ 20	≤ 20	≤ 20	[ns]
Far-field pattern FWHM	≤ 20	≤ 20	≤ 20	[°]
Cut-off wavelength (10 %)	-	-	3.7	[µm]
Detectivity	-	-	$\geq 0.5 \times 10^{11}$	[cmHz$^{1/2}$W^{-1}]
Emission bandwidth	0.5	0.5	-	[µm]
Detection range (50 % sensitivity)	-	-	2.85 - 3.65	[µm]

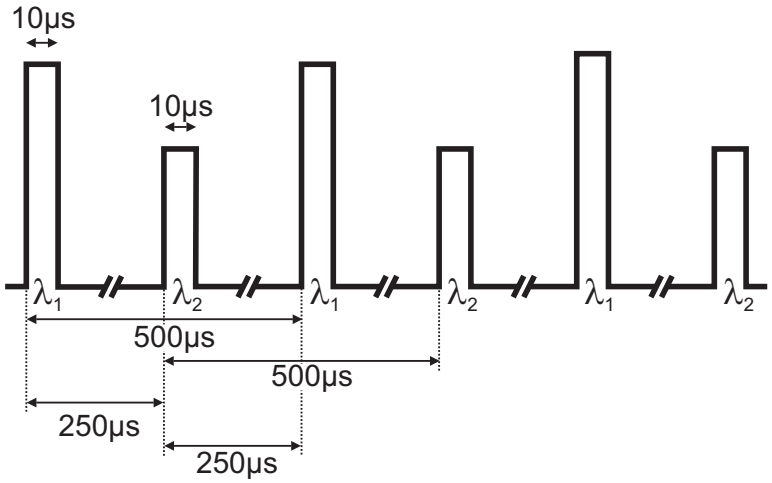

Figure 3.4: The drivers are synchronized and operate the 3.4 and 3.6 µm LED (λ_1 and λ_2) in an alternating pulse mode. The clock of one driver is inverted and used as a clock signal for the second driver.

3.2 Adaption of the sensor system

In the course of the present thesis the previously described sensor system was modified in such a way that the sample could be placed horizontally on a sample holder containing a 1.5 mm aperture. By means of an IR reflecting mirror positioned after the beamsplitter, the optical path was shifted 90° upwards and focussed on the aperture in the sample holder. Consequently, the photodiode was mounted above the sample platform. Figs. 3.5 and 3.6 show photographs of the adapted sensor setup and the new components used for the modification, respectively.

Apart from aforementioned modifications two NBP filters for CH_3 - antisymmetric and CH_3 - symmetric stretches at 3.383 and 3.483 µm were added to the filter wheels. Fig. 3.7 shows the

transmittance spectra of all six utilized NBP filters. In Tab. 3.2 the centre wavelengths of the NBP filters and their bandwidth are depicted. The utilized filters show transmittance bands that are overlapping with the peaks of interest (see Fig. 3.7). The centre wavelengths are slightly off the maximum CH_2 and CH_3 absorbance wavelengths but are close enough to yield almost the maximum possible transmittance. All filters have a bandwidth of less than or equal to 1 %, that is the percentage of the centre wavelength at full width at half the maximum peak transmission.

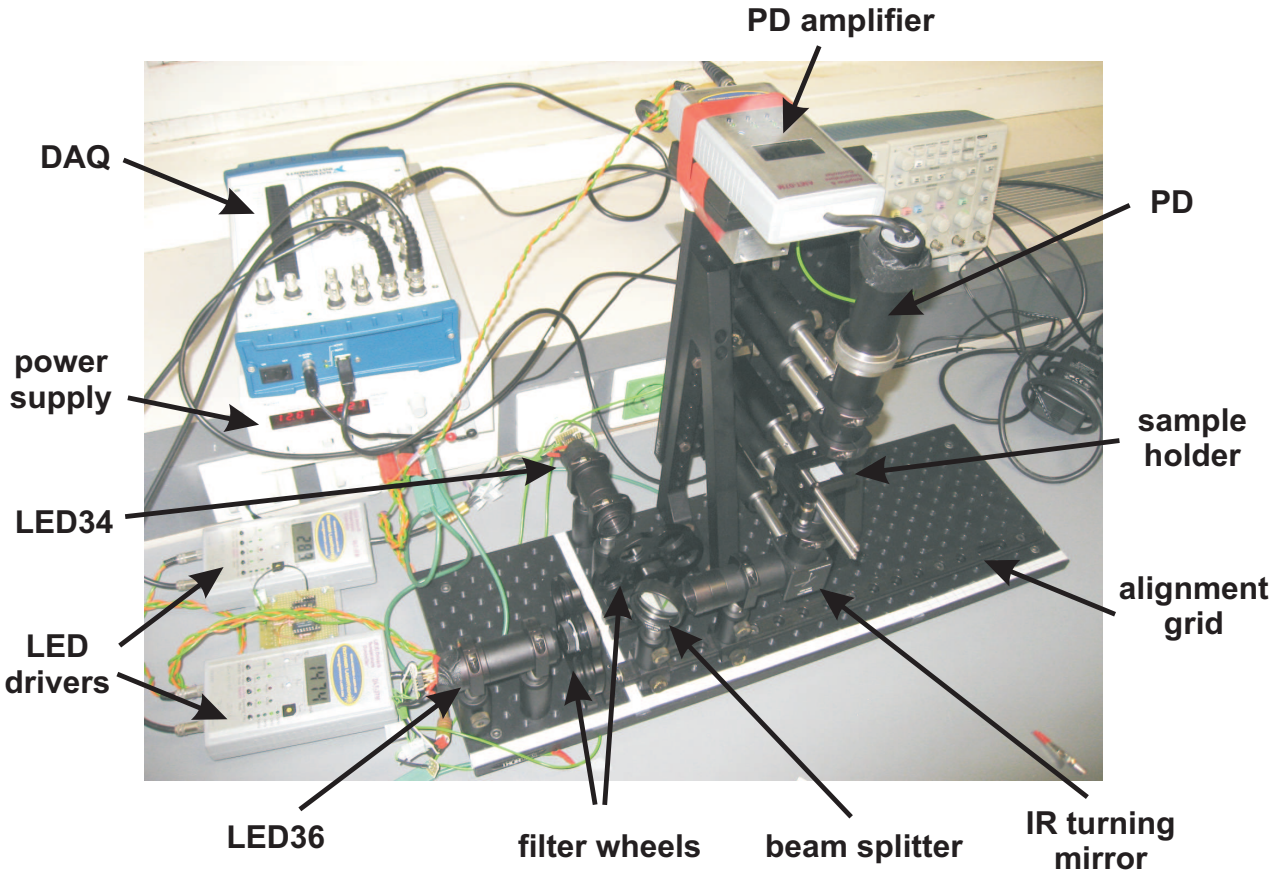

Figure 3.5: Photograph of the adapted sensor system. Compared to the old setup the light path is shifted 90° upwards by means of an IR turning mirror. The sample holder is now positioned in the vertical path. The photodiode (PD) is located inside the black vertical tube and the corresponding amplifier is attached to the top of the setup.

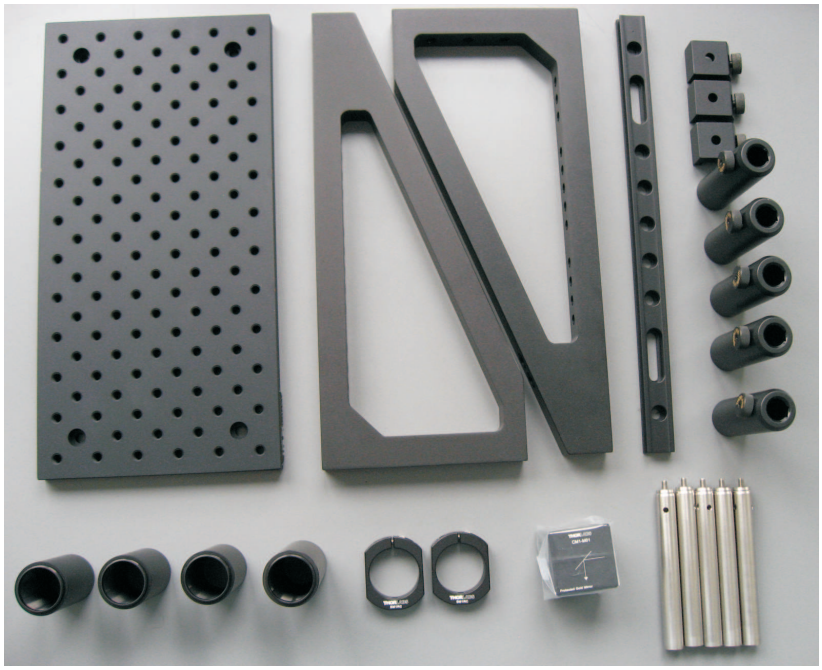

Figure 3.6: Additional components for the optical sensor setup. This includes an aluminum breadboard for vertical mounting (150 x 300 x 12.7 mm), two mounting brackets, an optical rail, several posts and post-holders, lens tubes plus appropriate holders and a turning mirror suitable for IR reflection.

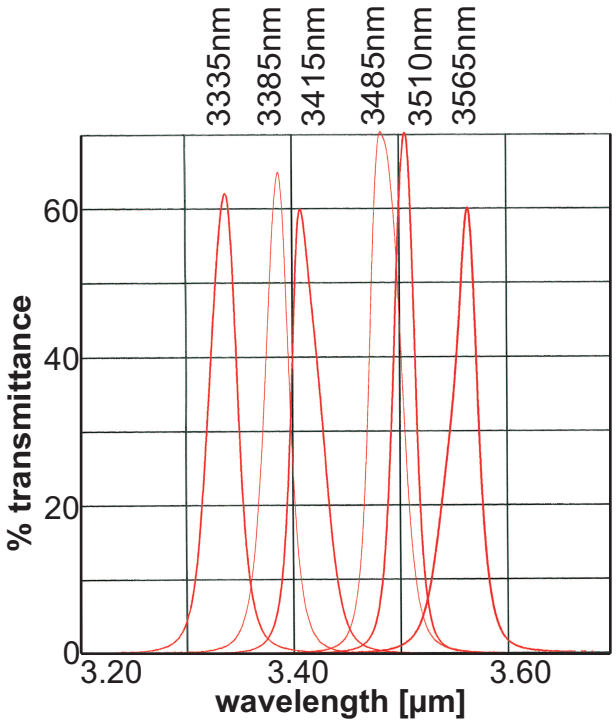

Figure 3.7: Transmittance spectra of the NBP filters for base-points (3335 and 3565 nm), CH_2-stretches (3415 and 3510 nm), and CH_3-stretches (3385 and 3485 nm).

Table 3.2: Centre wavelengths and bandwidths of the narrow-bandpass filters.

	Wavenumber [cm^{-1}]	Wavelength [µm]	Filter wavelength [µm]	Filter bandwidth [%]
Base point	3000	3.333	3.335	0.89
CH_3 antisymmetric	2958	3.383	3.385	1.0
CH_2 antisymmetric	2923	3.425	3.415	0.91
CH_3 symmetric	2871	3.484	3.485	1.0
CH_2 symmetric	2852	3.509	3.510	0.63
Base point	2800	3.572	3.565	0.77

3.3 Data acquisition

The measurement protocol required to obtain the IR absorbance of dried and suspended samples will be presented in chapters 4 and 6, respectively. However, the general data acquisition routine will be explained in this section. Although the quantity eventually determined is the absorptance, the absorbance and transmittance values can be easily derived from it (see chapter 2).

The procedure for a single measurement of a sample spot on an IR transparent slide is as follows:

The first filter set is selected from the filter-wheels, i.e. the filters for the base-points. Then the MATLAB script for signal recording can be started, upon which the photodiode output signal is recorded. A detailled view of such a single recorded pulse is shown in Fig. 3.8. The sample frequency is 1.25 Megasamples/s which results in a sample point every 0.8 µs. Also, the lower value is calculated when there is no LED pulsing (see Fig. 3.8). To extract information out of a pulse the highest value is discarded and the average of the four second highest values is used. This method resulted in pulse values with the lowest standard deviation. Depending on the presets a certain number of pulses for each LED34 and LED36 are sampled by the data acquisition board and averaged in order to enhance the accuracy of absorbtance values obtained. Usually, 100 pulses are sufficient for this purpose. This step yields a voltage at 3.335 and 3.565 µm which describes the baseline of the signal.

After this step the MATLAB program prompts the user to change the filter wheels to the next position and to continue the script. This time the current-to-voltage PD output signal at 3.415 and 3.510 µm is recorded (CH_2 - antisymmetric and CH_2 - symmetric stretch). The third step takes place similarly and yields the voltage at 3.385 and 3.485 µm (CH_3 - antisymmetric and CH_3 - symmetric stretch).

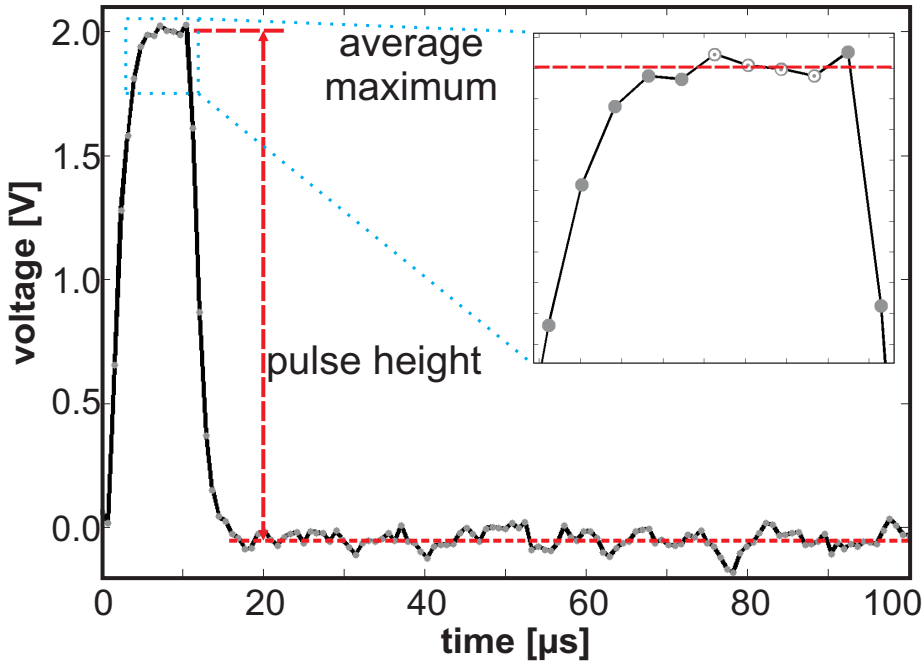

Figure 3.8: Recorded photodiode signal of a single LED pulse. Grey dots represent the sample points acquired with the data acquisition board. The average value of the four second highest sample points will be used with respect to the average lower level. This is the recorded voltage when the LEDs are not pulsing and it is determined by the photodiode dark current and noise.

By means of this procedure six photodiode output voltages are recorded and plotted. These values correspond to the light intensity after the measured sample at each of the six wavelengths. To obtain the absorbtance of a dried sample at the four CH_2 and CH_3 peak wavelengths, the transmittance difference of a sample-containing slide and an empty reference slide has to be compared (analogous for suspended cell samples, see Chapter 6). Hence, before measuring a spot on a cell sample the photodiode voltages of a reference slide have to be obtained which would represent a reference level of transmitted light. This level can be arbitrarily defined as 100 % transmittance. After that, the values for a sample spot are recorded, corresponding to $< 100\,\%$ transmitted light.

All measurement values are automatically saved in files and also stored in the MATLAB workspace for further processing. The MATLAB flow chart is shown in Fig. 3.9, all used routines can be found in the appendix.

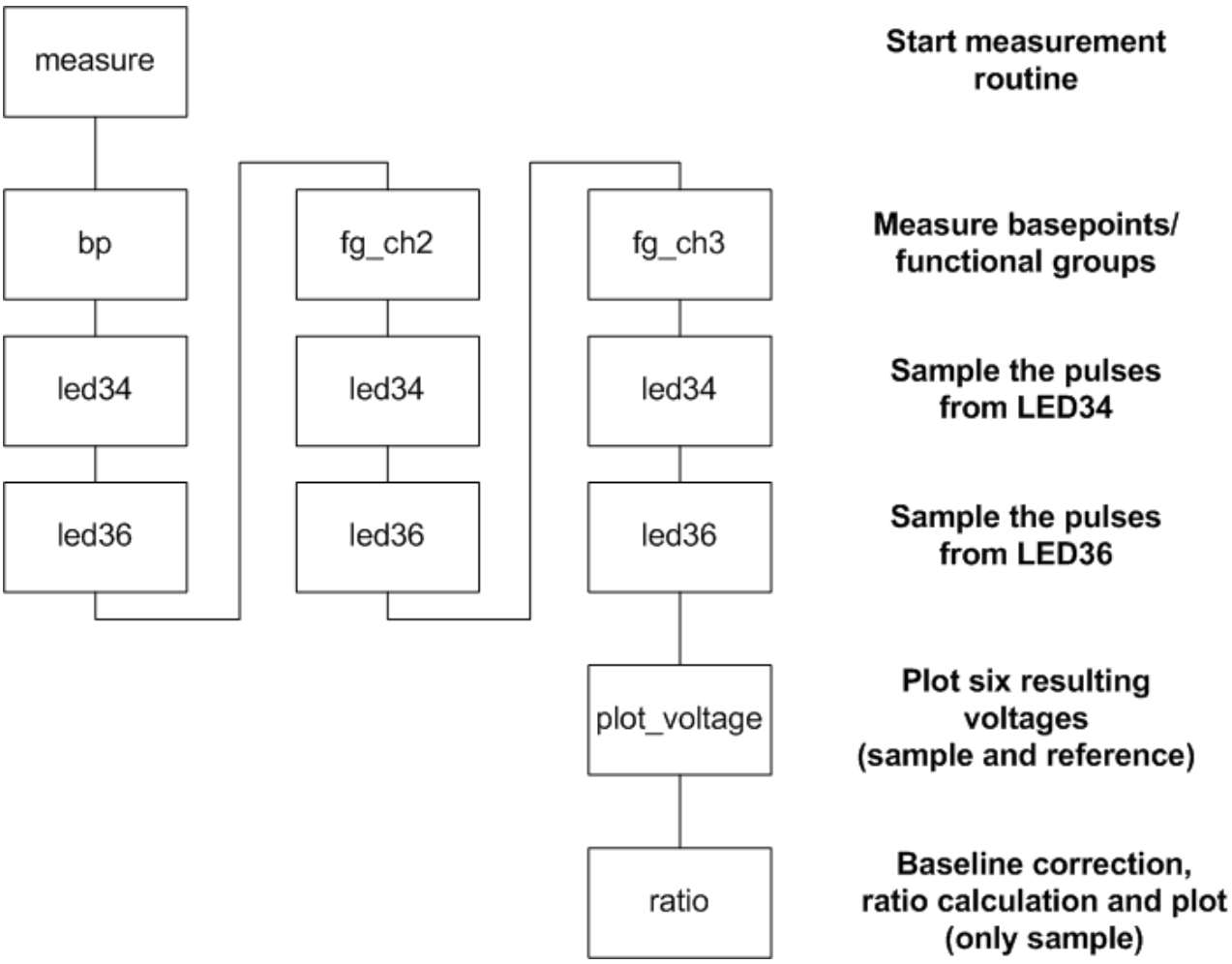

Figure 3.9: Sequential depiction of measurement, plotting, and calculation routines. They can be found in the appendix.

3.4 Baseline correction and ratio calculation

Measuring the sample and reference values corresponds to the determination of the light intensities $I_{Sample,\lambda}$ and $I_{Reference,\lambda}$, respectively. If the ratio of these two quantities is taken then the influence of the incident IR light and the sample slide is cancelled out. Hence, the result can be interpreted as the transmittance of only the sample. Exemplary values of the recorded PD voltages are depicted in Fig. 3.10. The figure also shows that the IR intensities emitted by the two LEDs are not equal, but deriving the percentage of absorbed light solves this problem.

The MATLAB routine '`ratio`' uses the recorded sample and reference values to baseline-correct the signal. That means it calculates the functional absorptance values and subsequently produces a ratio from the results, e.g. CH_2 - symmetric / CH_2 - antisymmetric stretches.

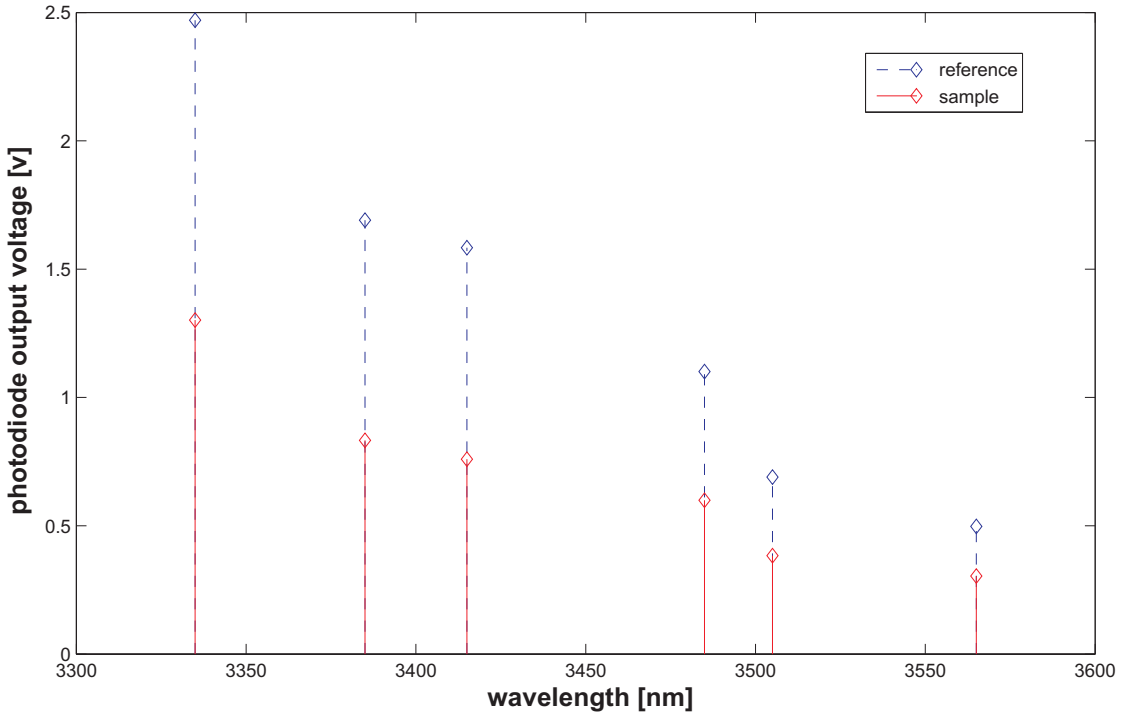

Figure 3.10: Typical photodiode output voltages for a reference slide and a dried cell sample. IR intensity of LED34 is higher than that of LED36, hence the ratio of sample and reference values is taken in the subsequent calculation steps.

In a first step the absorptance α in % at each wavelength is calculated (see Eq. 3.1) which gives the amount of absorbed IR light in percent per wavelength (see Fig. 3.11).

$$\alpha_\lambda = 100\% \cdot (1 - \frac{I_{Sample,\lambda}}{I_{Reference,\lambda}}) \tag{3.1}$$

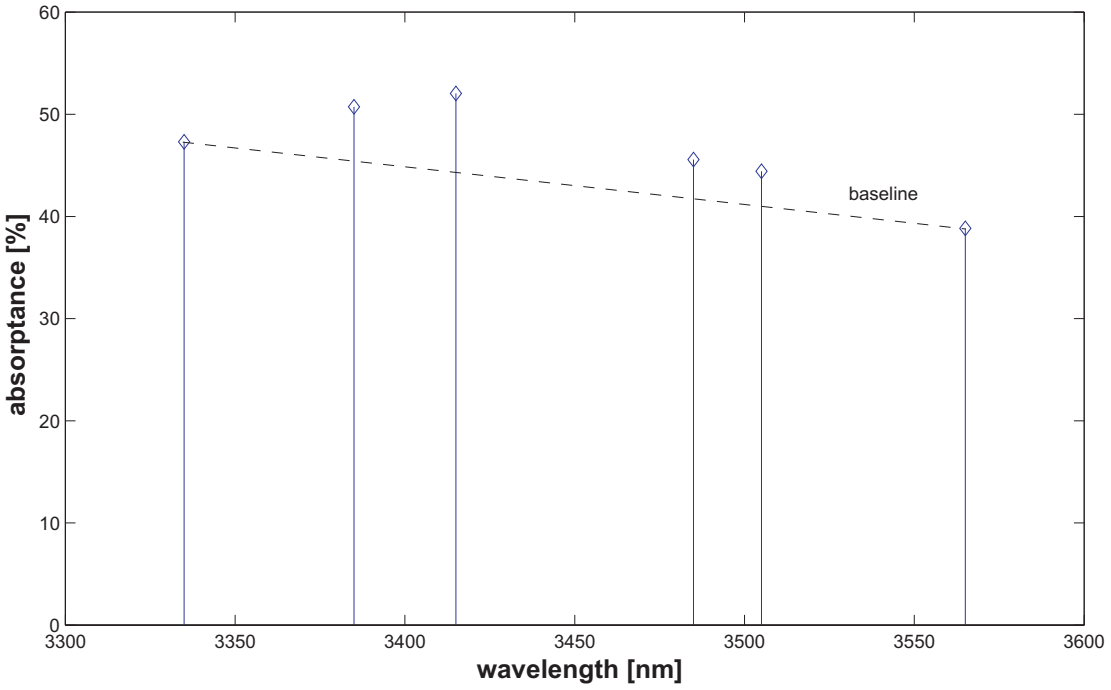

Figure 3.11: Absorptance in % calculated for above example. The baseline is constituted by the outer left and right values.

Then the baseline corrected absorptance at $\lambda = [3.385,\ 3.415,\ 3.485,\ 3.510]$ µm is calculated (see Eq. 3.2). The first terms are the absorptance difference between the absorptance at λ and the first base-point (3.335 µm). The wavelength distance between λ and the first base-point (λ - 3.335) is divided by the total distance between both base-points (3.565 - 3.335) and multiplied with the absorptance difference between both base-points ($\alpha_{3.565}$ - $\alpha_{3.335}$). Fig. 3.12 shows the baseline corrected absorptance for the above example.

$$\alpha_{\lambda,corrected} = \alpha_\lambda - \alpha_{3.335} + \frac{\lambda - 3.335}{3.565 - 3.335} \cdot (\alpha_{3.565} - \alpha_{3.335}) \tag{3.2}$$

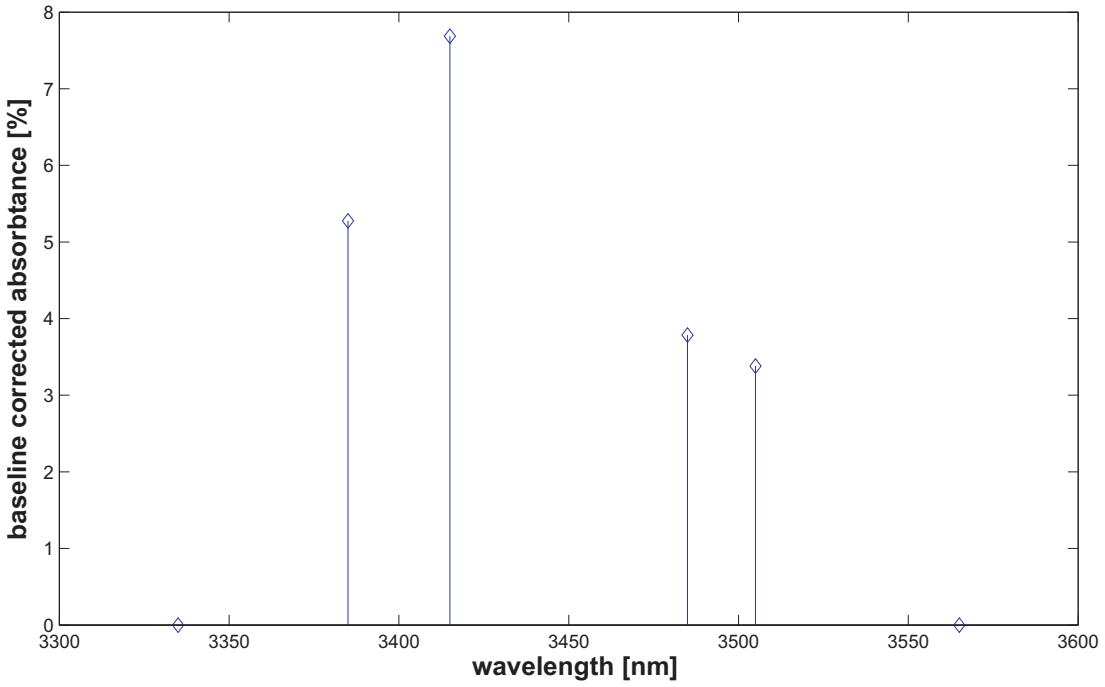

Figure 3.12: Baseline corrected absorptance in % calculated with above equations. The values for 3.335 and 3.565 µm are zero since they are base-points.

Previous calculations yielded the baseline corrected absorptance values for CH_2 and CH_3 stretches in %. Based upon these values any desired ratio can be evaluated. In the following chapter there will be a focus on the determination of the CH_2 - symmetric / CH_2 - antisymmetric stretch ratio (see Eq. 3.3).

$$\mathbf{ratio}_{CH_2sym\,/\,CH_2asym} = \frac{\alpha_{3.510}}{\alpha_{3.415}} \tag{3.3}$$

3.5 Sensor validation

The CH_2 - symmetric / CH_2 - antisymmetric stretch ratio of dried yeast samples has been recorded with the sensor system and compared with a commercial FTIR spectrometer (see Fig. 3.13). Both measurement systems yielded similar results.

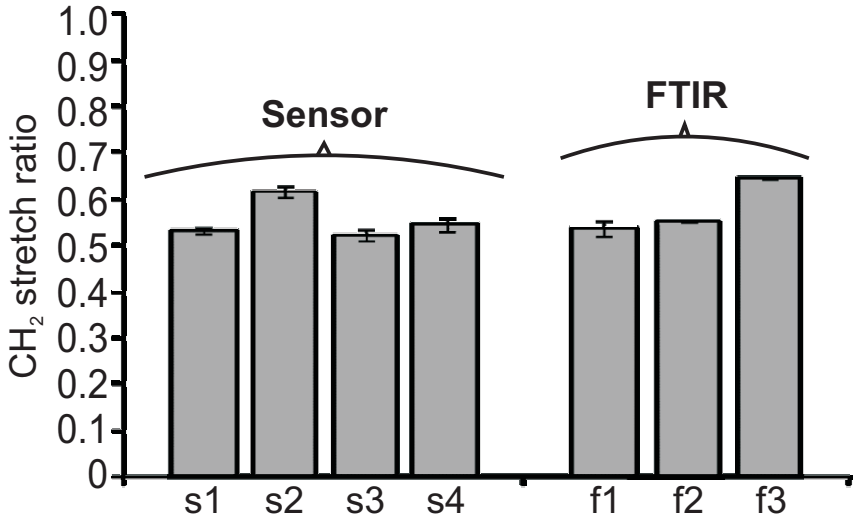

Figure 3.13: CH_2 - symmetric / CH_2 - antisymmetric stretch ratio measurements of four sample spots of dried yeast performed with the sensor system, each spot was recorded four times (left). Also, three sample spots were measured two times each with a commercial FTIR spectrometer (right). FTIR spectrometer settings were 1 mm beam diameter, 128 scans per spectrum at a resolution of 4 cm^{-1}. Grey bars show the mean values of the spots and error bars indicate the standard deviation.

4 Dried Cell Experiments

In this chapter the preparation and CH_2-stretch ratio measurement results of dried cell samples are presented. Cell samples include malignant and normal epithelial kidney cells (Caki-1 and MDCK, respectively) and human melanoma cell lines (M14 and A375) incubated with cisplatin. For epithelial kidney cells also the CH_3-stretch ratios are given.

4.1 Sample preparation

4.1.1 Epithelial kidney cells

Epithelial kidney cell lines MDCK (canine) and Caki-1 (human kidney carcinoma) were cultivated under the same conditions in monolayer on 1 mm thick CaF_2 slides at the Institute of Virology, Slovak Academy of Sciences, Bratislava, Slovakia. Temperature and CO_2 concentration were set to 37 °C and 5 %, culture medium consisted of DMEM (Dulbecco's Modified Eagle Medium), 2 mM L-glutamine, 10 % FCS (Fetal Calf Serum) and antibiotics (100 units/mL penicillin, 100 µg/mL streptomycin and 0.25 µg/mL Amphotericin B) all obtained from Lonza Bioscience. After cell attachment and formation of a confluent layer the slides were washed with PBS in order to remove culture medium. Slides were dried overnight and measured the next day.

For the preparation of MDCK / Caki-1 mixtures the two cell lines were grown seperately as described above. They were subsequently detached by means of trypsinization and their concentration in cells/mL was determined with a Coulter counter. Cell suspensions of Caki-1 and MDCK cells were then mixed in order to obtain desired mixing ratios. Mixes were pipetted onto CaF_2 slides in order to attach, followed by rinsing with warm PBS and drying.

Trypsinization is utilized for detaching cells from a substrate by means of the serin protease trypsin which cleaves the protein bonds between cells and substrate [9]. The trypsinization protocol for MDCK and Caki-1 is the following: Culture medium is removed and the attached cells are washed twice with PBS to remove components of the medium that inhibit trypsin, before trypsin is added. MDCK cells are incubated for 15 minutes at 37 °C and 5 % CO_2, Caki-1 are incubated at room temperature for two minutes. After that, cells are resuspended in DMEM containing 10 % FCS and carefully mixed by pipetting. Cells are then available in suspension and can be processed further, e.g. divided or counted and mixed as described above.

4.1.2 Melanoma cells

The human melanoma cell lines M14 and A375 used in the experiments originated from dentritic neural crest derived melanocytes found in the basal cell layer of the epidermis. Melanocytes are responsible for synthesizing the pigment melanin which protects skin from UV-radiation.

Melanoma cells were cultured at the Center of Pathophysiology, Infectiology & Immunology, Medical University of Vienna, Vienna, Austria. Culture medium consisted of RPMI 1640 (Roswell Park Memorial Institute medium), 2 mM L-glutamine, 10 % FCS, and antibiotics also obtained from Lonza Bioscience. Cells were grown attached to CaF_2 slides. Of each cell line a cisplatin incubated (20 µM, incubation time 16 hours) and a reference sample (0 µM) was prepared. Both cisplatin incubated and normal slides were rinsed with warm PBS, dried overnight, and measured the next day.

4.2 Measurement protocol

After switching on the equipment and the diode coolers, the LED driver currents were set. They were chosen in such a way that at the wavelength of 3.33 µm the photodiode output signal was below the clipping voltage of the photodiode (≈4 V) when no CaF_2 slide was present in the IR-beam, i.e. only the absorbtance of air was measured. Photodiode and LED parameters are shown in Tab. 4.1.

Table 4.1: Photodiode and LED parameters for dried cell experiments.

	LED34	LED36	Photodiode
current:	470 - 480 mA	1470 - 1480 mA	-
temperature:	10.4 °C	10.7 °C	20.7 °C

The IR transmittance of an empty CaF_2 reference slide was measured until the signal was stable, that is, no voltage drift occured, only fluctuations around a mean value with a standard error lower than 5 mV. For the actual measurements at first a spot on an empty slide was measured ten to fifteen times (reference value). Then a spot on a slide containing a cell monolayer was measured seven to ten times, in order to obtain an average value with acceptable standard deviation for the IR absorbtance. This procedure was repeated until four or five spots on the sample slide had been measured. All reference and sample absorptance values were stored. From these values the CH_2-stretch ratios of the cell samples were derived (see chapter 3).

4.3 Results and discussion

4.3.1 Epithelial kidney cells

Two sets of MDCK and Caki-1 cell samples were prepared and measured in order to compare their CH_2-stretch ratios. A sample set consisted of one or two sample slides. The time between preparation of set 1 and 2 was three months for MDCK and two weeks for Caki-1. In order to culture cell lines over a long time cell passaging is required [34]. That means cells are regularly split and a small part is transferred to another vessel where a new subculture is formed. This is done by removing the culture medium, followed by two washing steps with warm PBS, and by adding trypsin in order to detach cells adherent to a substrate (e.g. culture flask) before extracting a small amount of suspension containing cells. Subculturing is usually done every few days up to once a week depending on the growth rate. For each subculture step the passage number is set one higher. Since cells are subject to evolution it is possible that in every new generation genetic alterations occur. For instance, a high passage number (>100) is associated with protein expression changes in some cell lines [35]. However, the effect on CH_2-stretch ratio measurements will be negligible due to the relatively low number of cell passages between the measurements.

Depending on the confluency of cells on the sample slides the number of possible measurement spots varied but was usually around six. As mentioned, seven to ten measurements were done per spot and the resulting average value and standard deviation are shown. Spots with a standard deviation higher than 0.05 were discarded.

Also, sample slides with different mixture ratios of MDCK and Caki-1 were investigated and a brief comparison of the results regarding CH_3 stretch ratios (CH_3 - symmetric / CH_3 - antisymmetric) will be presented.

4.3.1.1 MDCK

Fig. 4.1 shows a photograph of dried MDCK cells cultured on a CaF_2 slide. The average size of spherical MDCK cells in suspension was 12 µm as determined with a coulter counter (see Fig. 4.2). However, when cells attach to a substrate they spread and therefore cover a larger area. The first sample set consisted of two sample slides, hence the number of usable measurement spots was larger than usual (ten) while the second sample set comprised six spots. Resulting values can be found in Fig. 4.3 and Tab. 4.2.

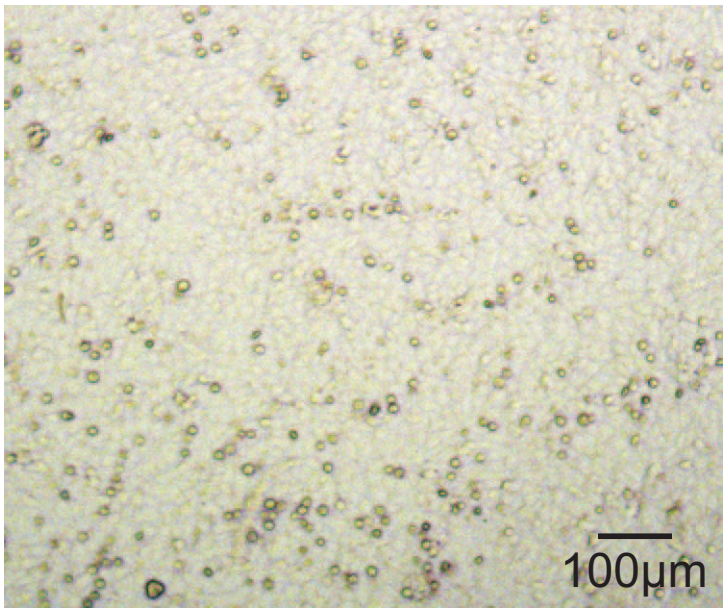

Figure 4.1: Photograph of dried MDCK cells attached to a CaF_2 slide.

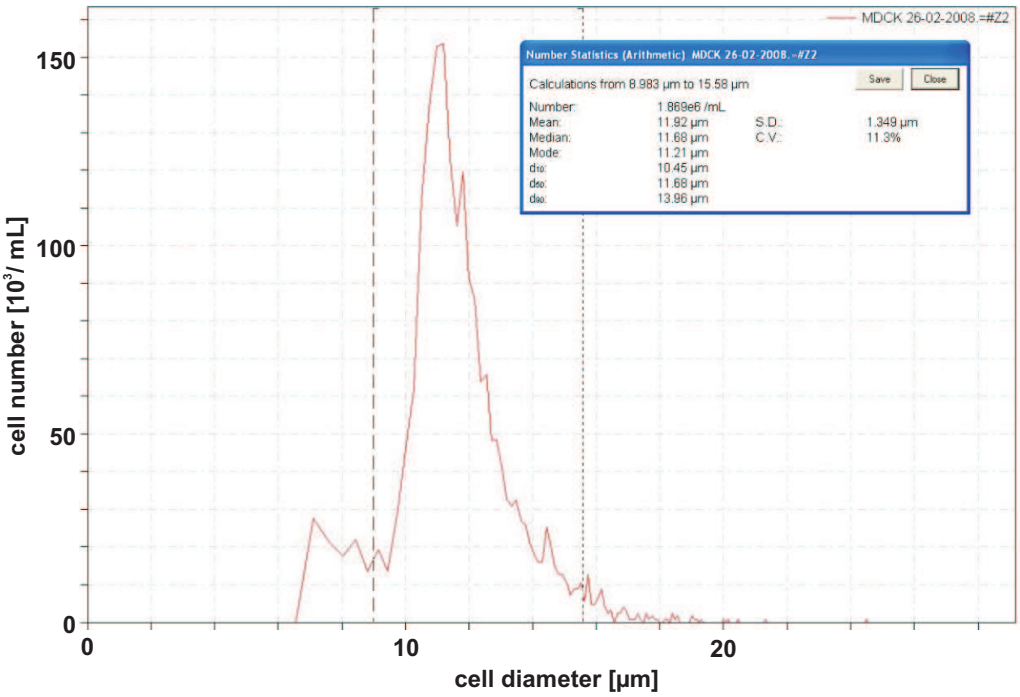

Figure 4.2: Results of MDCK cell counting and size determination with a coulter counter, mean cell size was 12 µm.

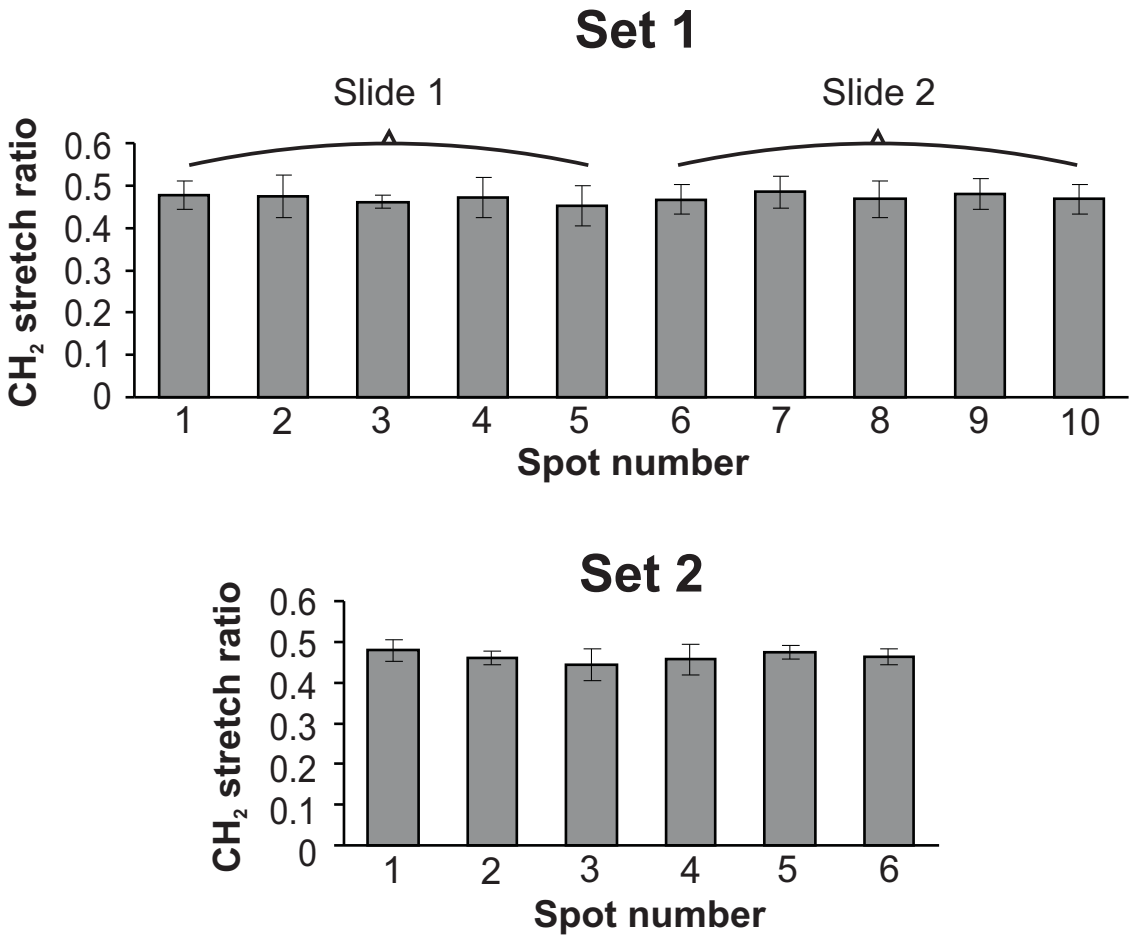

Figure 4.3: CH_2-stretch ratio of set 1 and set 2 of MDCK cells. The grey bars show the average ratio of seven to ten measurements per spot while the error bars indicate the standard deviation for the respective spot. The first sample set comprised more spots, because it consisted of two sample slides instead of one.

Table 4.2: Spot average and standard deviation of the CH_2-stretch ratio for the first and second set of MDCK.

	Set 1	Set 2
Spot 1	0.48 ± 0.03	0.48 ± 0.03
Spot 2	0.47 ± 0.05	0.46 ± 0.02
Spot 3	0.46 ± 0.01	0.44 ± 0.04
Spot 4	0.47 ± 0.05	0.46 ± 0.04
Spot 5	0.45 ± 0.05	0.47 ± 0.02
Spot 6	0.47 ± 0.03	0.46 ± 0.02
Spot 7	0.49 ± 0.04	
Spot 8	0.47 ± 0.04	
Spot 9	0.48 ± 0.04	
Spot 10	0.47 ± 0.04	

4.3.1.2 Caki-1

Fig. 4.4 shows a photograph of dried Caki-1 cells grown attached to a CaF_2 slide, the average cell size in suspension was about 17 µm (see Fig. 4.5). The number of measurement spots for each sample set was five, resulting values can be found in Fig. 4.6 and Tab. 4.3.

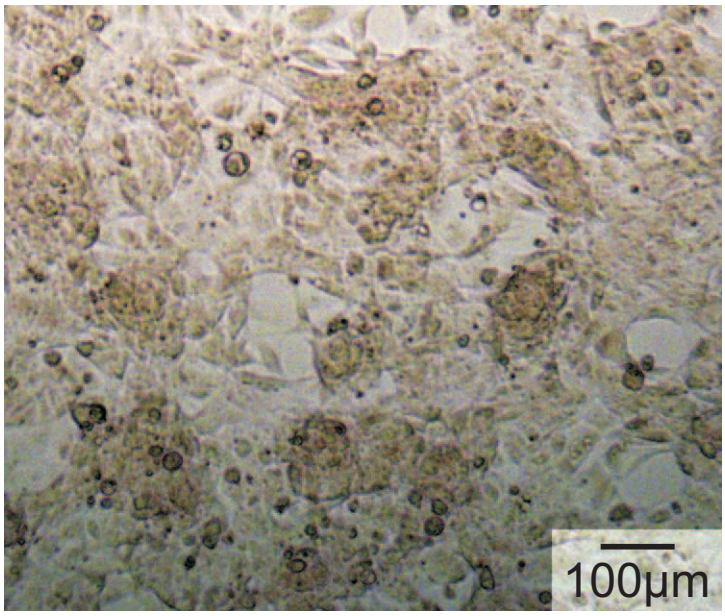

Figure 4.4: Photograph of dried MDCK cells on a CaF_2 slide.

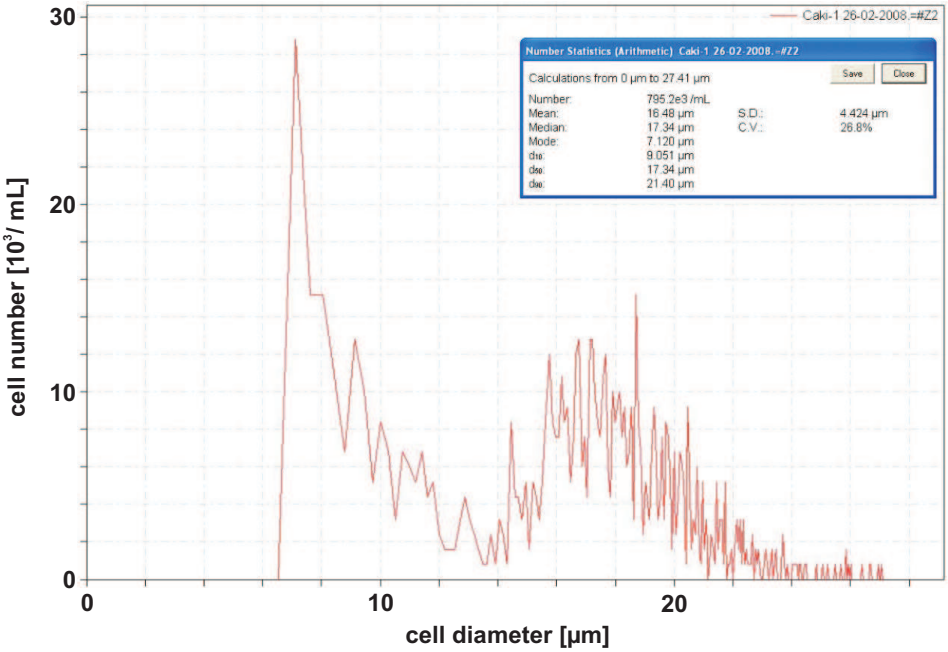

Figure 4.5: Results of Caki-1 cell counting and size determination with a coulter couter. Average cell size was 16.5 µm. The peak at 7 µm represents a coulter counter specific artefact that occurred in all measurements.

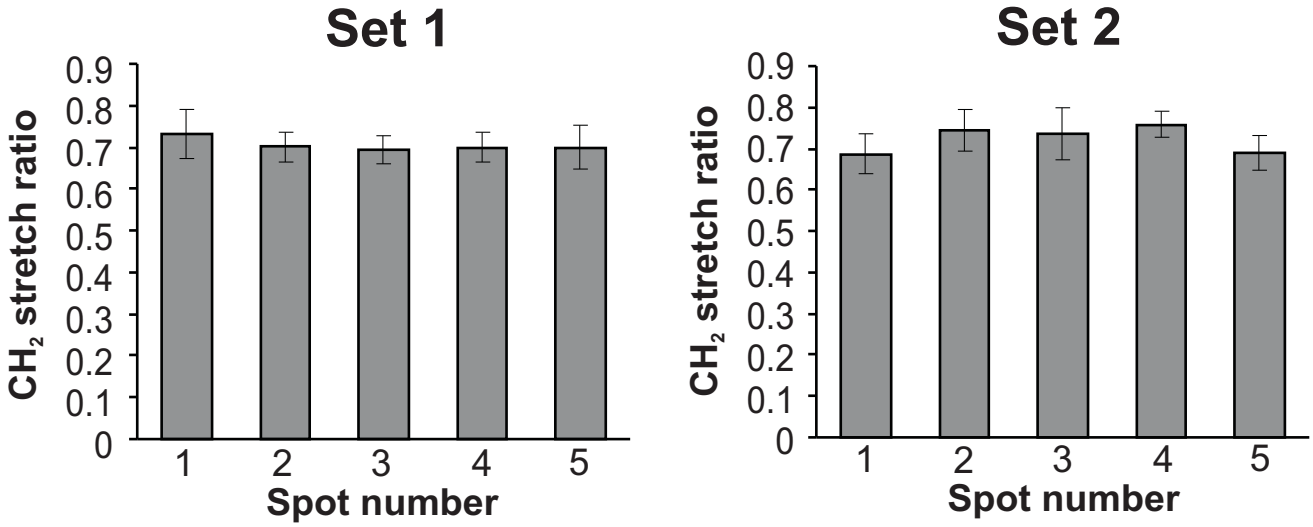

Figure 4.6: CH_2-stretch ratio of set 1 and set 2 of Caki-1 cells. The grey bars show the average ratio for each spot while the error bars indicate the standard deviation.

Table 4.3: Spot average and standard deviation of the CH_2-stretch ratio for the first and second set of Caki-1.

	Set 1	Set 2
Spot 1	0.73 ± 0.06	0.69 ± 0.05
Spot 2	0.70 ± 0.04	0.74 ± 0.05
Spot 3	0.69 ± 0.03	0.74 ± 0.06
Spot 4	0.70 ± 0.03	0.76 ± 0.03
Spot 5	0.70 ± 0.05	0.69 ± 0.04

4.3.1.3 Comparison of Caki-1 and MDCK

In Fig. 4.7 and Tab. 4.4 the averaged CH_2-stretch ratios of the first and second set of each MDCK and Caki-1 are compared. The CH_2-stretch ratio for the Caki-1 cell line is significantly higher than for the MDCK cell line, average values are 0.71 and 0.47, respectively. As described in section 2.3 the findings of *Driesche et al.* (compare Fig. 2.12 and Ref. [13]) suggested that the CH_2-stretch ratio increases for Caki-1 with respect to MDCK cells, which is in accordance with the sensor measurements.

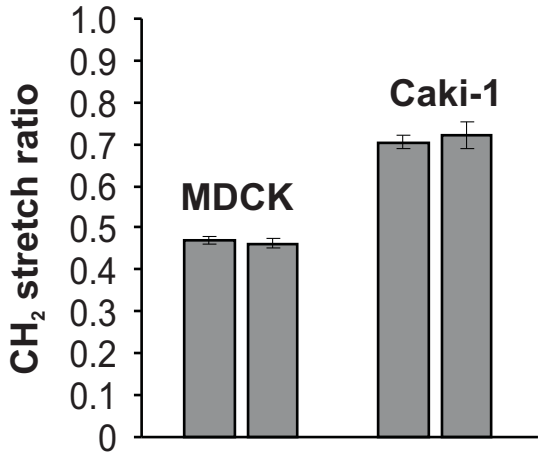

Figure 4.7: Average CH_2-stretch ratios for both sets of MDCK and Caki-1. The grey bars indicate the average ratio of all spots of each sample set, the error bars indicate the standard deviation.

Table 4.4: Sample set average and standard deviation for all spots of both sets of MDCK and Caki-1.

		CH_2-stretch ratio
MDCK	Set 1	0.47 ± 0.01
MDCK	Set 2	0.46 ± 0.01
Caki-1	Set 1	0.71 ± 0.01
Caki-1	Set 2	0.72 ± 0.03

4.3.1.4 Mixture of Caki-1 and MDCK

Besides measuring the CH_2-stretch ratio of pure Caki-1 and MDCK, also mixtures have been investigated. The experiments were performed in order to determine if a distinction between those mixtures is feasible.

In Fig. 4.8 a photograph of a mixture of 50 % Caki-1 and 50 % MDCK is shown, which means that the cell concentration of Caki-1 and MDCK was the same. Fig. 4.9 shows the average CH_2-stretch ratio for all Caki-1 / MDCK mixing ratios. A distinction between different Caki-1 / MDCK mixes by means of measuring the CH_2-stretch ratio is possible (see Tab. 4.5). The higher standard deviation of the 80 / 20 and 20 / 80 mixes is most likely due to the non-uniform distribution of MDCK and Caki-1 on the sample slides. That means that there are for instance spots with a higher concentration of Caki-1, which yield a higher stretch ratio than spots where MDCK are abundant. The cell distribution as shown in Fig. 4.8 for example comprises more Caki-1 than MDCK cells. Averaging of multiple spots, however, results in a statistical mean value of the CH_2-stretch ratio that can be used to characterise the respective mixing ratio.

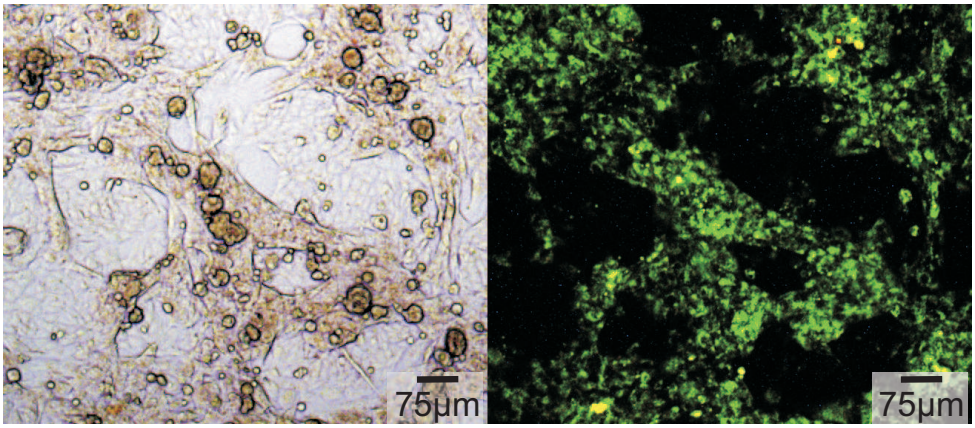

Figure 4.8: Photograph of 50 % Caki-1 and 50 % MDCK mixture (left). Caki-1 have been stained with a fluorescent viability stain (DiO, see [36]) that binds to phospholipid bilayer membranes. Stained Caki-1 cells can be clearly distinguished from the MDCK cells in the mixture (right). Samples that had been stained previously were not measured in order to avoid compromised results.

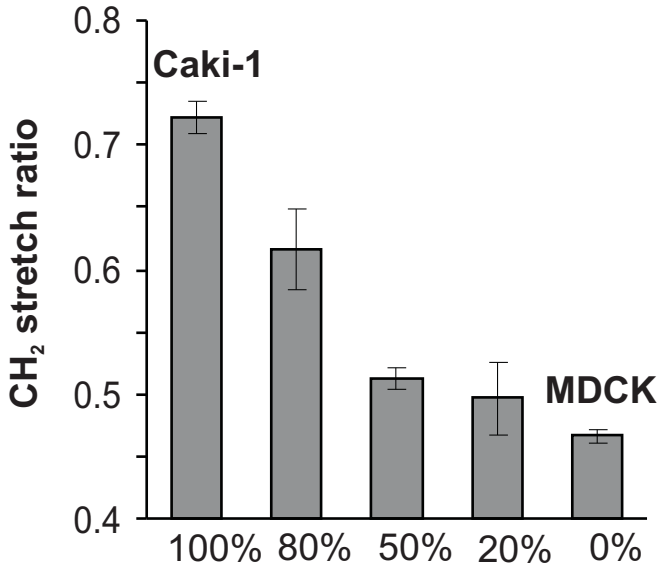

Figure 4.9: CH_2-stretch ratio for mixtures of MDCK and Caki-1. The grey bars indicate the average ratio of all sample sets measured for the corresponding mix ratio, the error bars indicate the standard deviation.

Table 4.5: Average values and standard deviation for MDCK and Caki-1 mixtures. The values of 100% Caki-1 and 100% MDCK are the results from section 4.3.1.3, while the other ratios were obtained from one sample set each.

Caki-1 / MDCK	CH_2-stretch ratio
100 / 0	0.71 ± 0.01
80 / 20	0.62 ± 0.03
50 / 50	0.51 ± 0.01
20 / 80	0.50 ± 0.03
0 / 100	0.47 ± 0.01

4.3.1.5 CH_3-stretch ratio

Besides the CH_2-stretch ratio we also investigated the feasability of distinguishing normal and malignant cells by comparing the CH_3-stretch ratio (CH_3 - symmetric / CH_3 - antisymmetric stretch ratio). CH_3 stretch ratios have been observed for MDCK, Caki-1, and mixtures of both, as shown in Figs. 4.10 - 4.11 and Tabs. 4.6 - 4.7. Analogous to the CH_2-stretch ratio, Caki-1 cell lines exhibit a much higher CH_3-stretch ratio compared to MDCK, with an average of 1.22 compared to 0.63, respectively.

However, a clear distinction between 50 / 50 and 20 / 80 Caki-1 / MDCK mixing ratio was not obtained. As described above, the higher standard deviation of the 80 / 20, 50 / 50 and 20 / 80 mixes was due to an uneven distribution of Caki-1 and MDCK cells. If the distribution is highly non-uniform or locally concentrated, it is possible that averaging of all recorded spots on the sample slide does not yield the desired statistical average values.

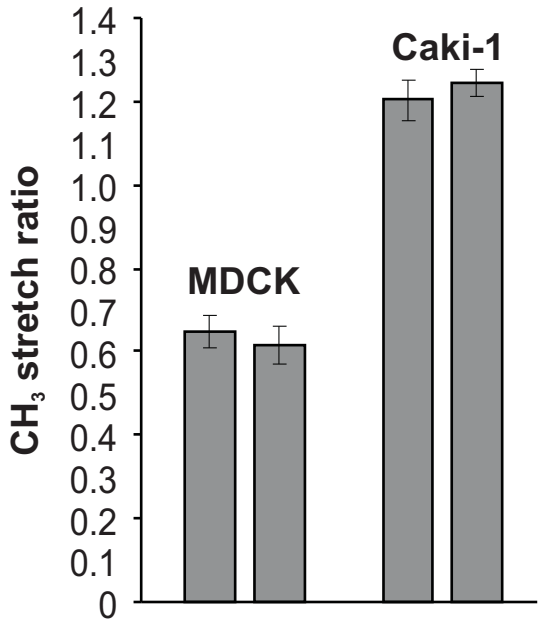

Figure 4.10: Average CH_3-stretch ratios for both sets of MDCK and Caki-1. The grey bars indicate the average ratio of all spots measured for a sample set, the error bars indicate the standard deviation. Two sample sets of each MDCK and Caki-1 were measured.

Table 4.6: Sample set average and standard deviation of the CH_3-stretch ratio for both sets of MDCK and Caki-1.

		CH_3-stretch ratio
MDCK	Set 1	0.65 ± 0.04
MDCK	Set 2	0.62 ± 0.04
Caki-1	Set 1	1.20 ± 0.05
Caki-1	Set 2	1.24 ± 0.03

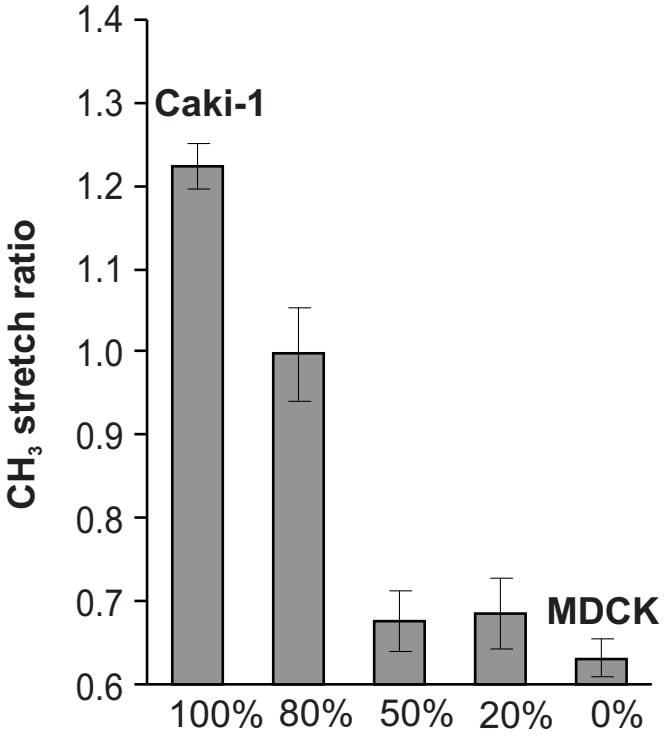

Figure 4.11: CH_3-stretch ratio for mixtures of MDCK and Caki-1. The grey bars indicate the average ratio of all sample sets measured for the corresponding mix ratio, the error bars indicate the standard deviation.

Table 4.7: Average values and standard deviation of the CH_3-stretch ratio for MDCK and Caki-1 mixtures.

Caki-1 / MDCK	CH_3-stretch ratio
100 / 0	1.22 ± 0.03
80 / 20	1.00 ± 0.05
50 / 50	0.68 ± 0.04
20 / 80	0.69 ± 0.04
0 / 100	0.63 ± 0.02

4.3.2 Cisplatin incubated melanoma cells

The CH_2-stretch ratio of two melanoma cell lines (M14 and A375) has been compared for both untreated cells and cells incubated with cisplatin. Two untreated cell sample sets were prepared and measured two weeks after each other. The ratio is lower for the M14 cell line with respect to the A375. A comparison of untreated and cisplatin incubated cells shows that the CH_2-stretch ratio significantly decreased for cisplatin treated cells. Tab. 4.8 and Figs. 4.12 - 4.13 show the average results.

From the data presented by *Zwielly et al.* we found that cisplatin-sensitive melanoma cells (GA) exhibit a lower CH_2-stretch ratio than cisplatin-resistive GAC cells [8]. Our measurements showed that treatment with 20 µM cisplatin for 16 hours decreased the CH_2-stretch ratio of M14 and A375, which indicated that both cell lines responded to the drug and hence suggests that apoptosis was induced.

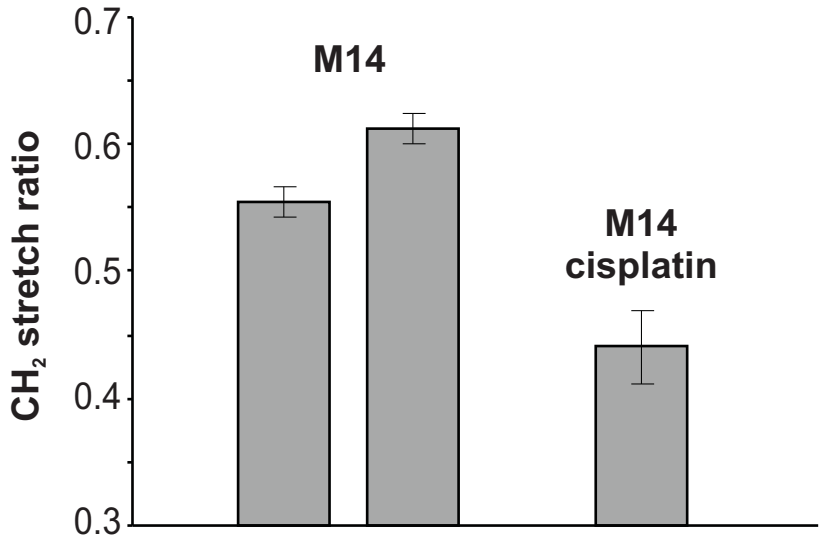

Figure 4.12: CH_2-stretch ratio for two sets of normal and one set of cisplatin incubated M14 melanoma cells. Cisplatin concentration was 20 µM, incubation period was 16 hours. The bars show the average value of all spots measured on a set, the error bars indicate the standard deviation.

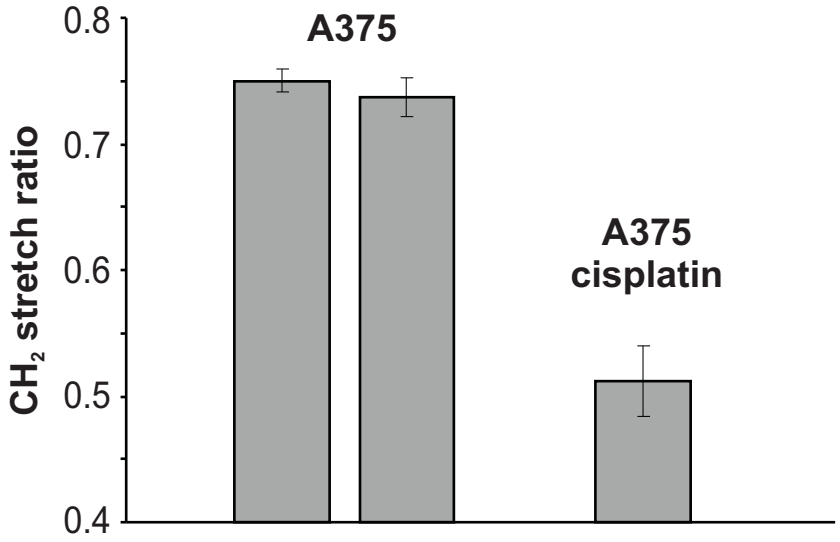

Figure 4.13: CH_2-stretch ratio for two sets of normal and one set of cisplatin incubated A375 melanoma cells. Cisplatin concentration was 20 µM, incubation period was 16 hours. The bars show the average value of all spots measured on a set, the error bars indicate the standard deviation.

Table 4.8: Average values and standard deviation of the CH_2-stretch ratio for normal and cisplatin incubated melanoma cell lines M14 and A375.

	CH_2-stretch ratio
M14 set 1	0.56 ± 0.01
M14 set 2	0.61 ± 0.01
M14 cisplatin	0.44 ± 0.03
A375 set 1	0.75 ± 0.01
A375 set 2	0.74 ± 0.02
A375 cisplatin	0.51 ± 0.03

5 Chip Development

In order to conduct CH_2- and CH_3-stretch ratio measurements for cell suspensions, a microfluidic device is required. Theoretical considerations as well as the design and fabrication of a chip comprising measurement chambers for liquid samples will be described in the following sections.

5.1 Chip design

IR absorbance measurements of dried cells (see chapter 4) require a rather elaborate and time consuming sample preparation, i.e. the growth of a confluent cell monolayer on the CaF_2 slides and a subsequent drying step to overcome the strong absorbance of water in the 2800 - 3000 cm^{-1} region. If the thickness of the water layer is sufficiently thin, the absorbance is reduced and hence the resulting photodiode output signal can become sufficiently high. Thus, cells suspended in water and confined to a microchamber made of infrared transparent material will allow for IR absorbance measurements.

In contrast to the measurement of dried cells, which are obviously not alive, the proposed method offers the additional advantage of live cell measurements. While dehydration quickly kills cells, it is possible to keep them alive in PBS during the measurements. PBS is a water-based salt solution that is used to maintain a constant pH and osmolarity. The salts present in the solution do not interfere with the measurements of CH_2 and CH_3 absorbance peaks in the IR spectrum. Using cell culture medium as suspension liquid is not recommended since it contains carbon chains from e.g. sugars and aminoacids which would definitely influence the absorbance spectrum if not render the measurements impossible. Thus, cell samples have to be free from culture medium residues.

While the reference for dried cell measurements was an empty, clean CaF_2 slide, it would now be the CaF_2 layers of the confining chip structure and the suspension liquid without cells. The cells used for the present work are about 15 µm in diameter, therefore a chamber height of about 20 µm would be necessary. That way the formation of a confluent cell monolayer and the reduction of empty space, that is PBS solution without cells, could be achieved. In a chamber with an increased height the absorbance of the surrounding water would become too high, while in a too thin chamber larger cells could clog. In the following sections the design steps in order to find a proper layout for the chip and the microchamber are described.

5.1.1 Absorbance measurements of water and heavy water

Venyaminov and Prendergast have measured the molar absorptivity or molar extinction coefficient E^{λ} of H_2O and the isotope D_2O (deuterium oxide) in the 1000 - 4000 cm^{-1} spectral region (2.5 - 10 µm) by means of FTIR [37]. In Fig. 5.1 the molar absorptivities of H_2O and D_2O are depicted for comparison, while the values at the six wavelengths of the present sensor system are shown in Tab. 5.1. The amount of light transmitted through a layer of water or heavy water can be calculated using Eq. 5.1:

$$T = 100\% \cdot 10^{A} = 100\% \cdot 10^{E^{\lambda} \cdot C \cdot l} \tag{5.1}$$

T is the transmittance in %, A the absorbance, E^{λ} is the molar extinction coefficient, C is the concentration of H_2O or D_2O (i.e. 55.14 M and 55.34 M, respectively) and l is the thickness of the layer.

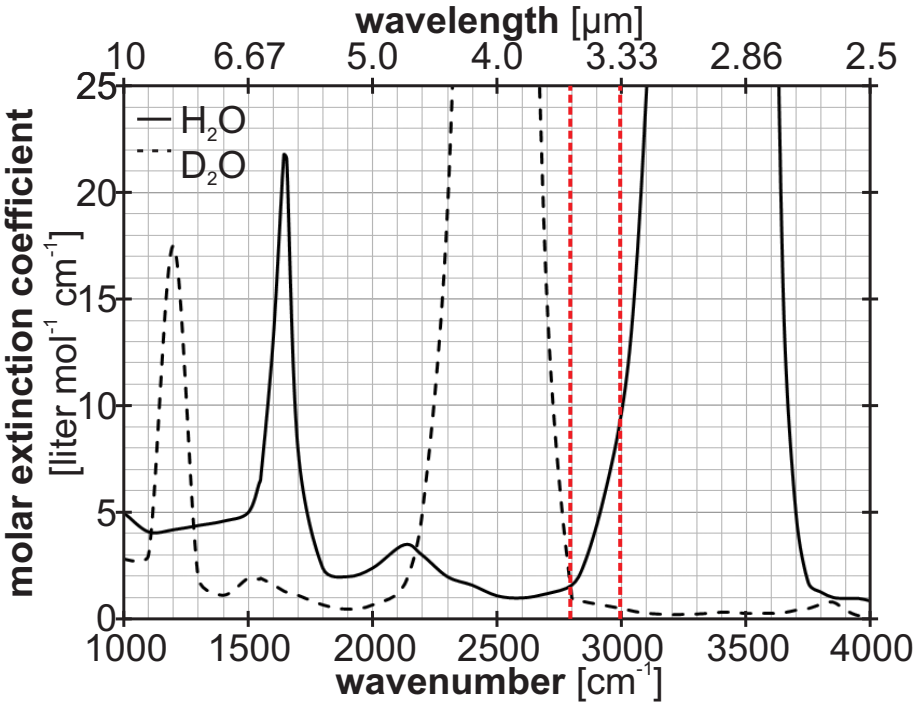

Figure 5.1: Molar absorptivity of water and heavy water for the 1000 - 4000 cm^{-1} range. Data extracted from [37]. The region between the dashed vertical lines represents the region of interest. As can be seen, the molar absorptivity of D_2O is significantly lower than the one of H_2O, especially at 3.33 µm (3000 cm^{-1}).

Table 5.1: Molar absorptivity of water and heavy water.

	Wavenumber [cm^{-1}]	Filter wavelength [µm]	Molar absorptivity (H_2O) [$M^{-1} \cdot cm^{-1}$]	Molar absorptivity (D_2O) [$M^{-1} \cdot cm^{-1}$]
Base point	3000	3.335	9.7	0.48
CH_3 antisymmetric	2958	3.385	6.5	0.6
CH_2 antisymmetric	2923	3.415	5.3	0.65
CH_3 symmetric	2871	3.485	3	0.72
CH_2 symmetric	2852	3.510	2.6	0.8
Base point	2800	3.565	1.6	1

As can be seen in Fig. 5.1, heavy water transmits more of the incident light than normal water in the lower wavelength region (3.33 µm). Assuming that cells could survive in deuterium oxide based PBS for a short time, it is possible to use pure or diluted PBS-D_2O as cell suspension liquid. Unfortunately, later measurements showed that the amount of absorbed IR-radiation increased over time for D_2O and mixtures of D_2O and H_2O. This means that the output voltage decreased for all six wavelengths. The trend for a mixture of 50 % D_2O and 50 % H_2O at 3.33 µm is shown in Fig. 5.2. The voltage decreased by an average of 0.36 mV/min or 43 mV within two hours of measurements. The voltage drop was higher at the 3.33 µm wavelength than at 3.6 µm, which suggests an increasing influence of H_2O. The reason might be the reaction of D_2O and H_2O in order to generate DOH until an equilibrium state between those three compounds is reached [38]. Also, 100 % D_2O is apparently not absolutely pure, since aforementioned behaviour was also observed here. To improve the stability of this method, more research is projected.

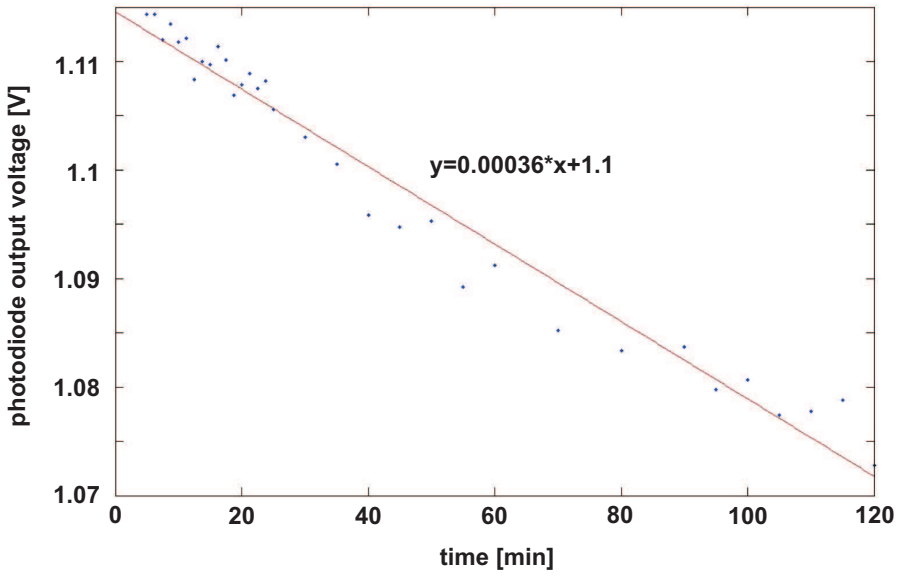

Figure 5.2: Output voltage drop for a mixture of D_2O and H_2O, 50 % each. Within two hours the voltage decreased by 43 mV.

5.1.2 Test setup

Before the decision to fabricate a microfluidic chip, experiments with a 'test chip' have been conducted. This chip was composed of two borosilicate glass microscopy slides and teflon strips, normally used for waterproof sealing of pipes, or scotch tape strips. The SiO_2 slides were 140 µm thick, and according to the manufacturers, the thicknesses of the teflon and scotch tape were 75 µm and 58 µm, respectively. Strips were placed between the glass slides and the edges were glued together with commercial nail polish. Hence, a chamber-like structure was produced which was filled with H_2O or D_2O and afterwards sealed with lacquer (see Fig. 5.3). The thin slides also compensated for the somewhat worse transmittance of SiO_2 compared to CaF_2 in the 3.33 to 3.6 µm wavelength range. But due to the large chamber height the signal for H_2O was too low, therefore only measurements with D_2O could be conducted.

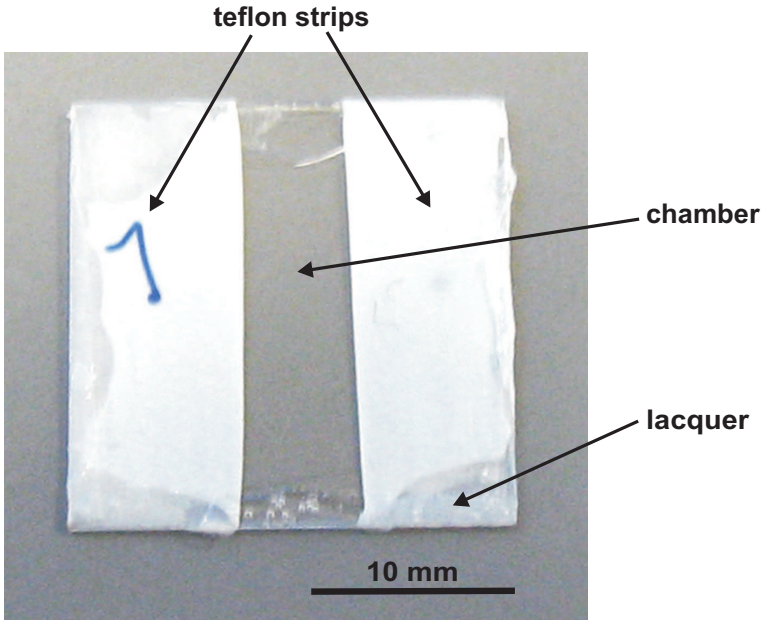

Figure 5.3: Photograph of the test chip setup.

For suspended cell measurements with the current LED and PD parameters as well as H_2O-PBS as suspension liquid, the fabrication of a microfluidic device with a smaller chamber height was indicated. In order to find the optimal chamber height, another test chip setup was arranged, which consisted of two SiO_2 slides as above but only a single scotch tape strip on one side of the chip. Hence, with this chip a layer of H_2O with gradually increasing thickness could be created. Consequently, the photodiode voltage decreased when a spot with a thicker H_2O layer was measured. The minimal voltage was chosen to be 150 mV and compared with the voltage measured for two empty glass slides. The resulting transmittance of H_2O at 3.33 µm was about 8 %, which corresponded to an approximately 21 µm thick H_2O layer (see Eq. 5.1). The resulting transmittance for a chamber height of 21 µm is shown in Tab. 5.2. These results show that for the utilized LEDs and PD at the wavelengths of interest a chamber height of 20 - 22 µm would be sufficient to conduct measurements with cells suspended in PBS.

Table 5.2: Transmittance differences between a 21 µm thick layer of water and heavy water.

	Wavenumber [cm^{-1}]	Filter wavelength [µm]	Transmittance (H_2O) [%]	Transmittance (D_2O) [%]
Base point	3000	3.335	7	88
CH_3 antisymmetric	2958	3.385	17	85
CH_2 antisymmetric	2923	3.415	24	84
CH_3 symmetric	2871	3.485	45	83
CH_2 symmetric	2852	3.510	50	81
Base point	2800	3.565	65	77

5.1.3 Chip layout

Since the purpose of the microfluidic chip are IR-absorption measurements of cells supended in PBS, several design issues have to be considered. The substrate must be transparent in the infrared and visible light region to allow for IR measurements and optical inspection. The fluidic chambers on the chip should comprise enough space to allow the measurement of multiple sample spots. Suspended cells inside the measurement chamber should form a monolayer, which requires a proper chamber height. Also, the IR absorption of the suspension liquid that increases with the chamber height has to be taken into account.

Thus, the chip consists of two sandwiched infrared transparent CaF_2 wafers, each with a thickness of 1 mm, and in between three fluidic chambers. The measurement chambers are made of SU-8, a negative photoresist that is widely used for MEMS and microfluidic devices [39, 40]. To facilitate monolayer formation and at the same time prevent channel clogging and strong IR absorption due to water, the desired chamber height was selected to be between 20 and 22 µm. Moreover, a 3.5 mm diameter chamber is sufficiently large for the IR-measurements of five different spots, since the diameter of the IR beam is only about 1.5 mm. With this diameter the obtained chamber volume is approximately 0.2 µL. A schematic and a photograph of the chip are depicted in Figs. 5.4 and 5.5, respectively .

The inlet and outlet holes positioned on each side of the chamber are used to fill the chip with cell suspensions (see Fig. 5.6). In order to prevent evaporation of the liquid the holes are sealed with PDMS (poly-dimethyl-siloxane) strips that stick to the CaF_2 surface by themselves, making a device holder obsolete.

Microfluidic simulations with COMSOL were done beforehand in order to find a chamber design with very little dead space when filled with cells suspended in liquid (see Fig. 5.7). The lithography masks to selectively expose regions of the SU-8 photoresist were drawn with AUTOCAD (see Appendix, Figs. A - C).

CaF_2 was the substrate material of choice, since its transmittance in the IR wavelength region from 2800 to 3000 cm^{-1} is over 95 % compared to 83 - 93 % for silicon dioxide SiO_2 glass of the same thickness [41]. Devices comprising a CaF_2 substrate and SU-8 fluidic structures for IR spectroscopy applications have also been developed and employed by [42, 43, 44].

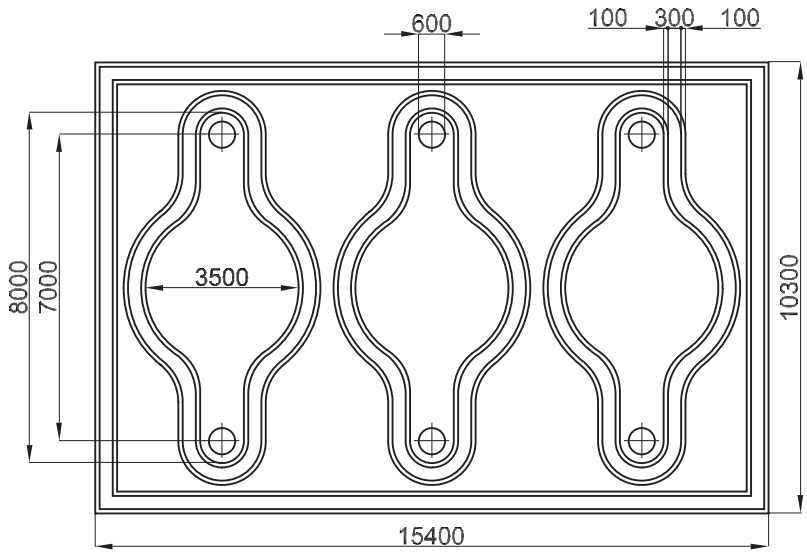

Figure 5.4: Chip layout. All measures in µm. The 100 µm thin side wall structures consist of exposed SU-8 while the 300 µm space between is filled with unexposed, soft SU-8, as described in section 5.2.

Figure 5.5: Photograph of the IR-measurement chip.

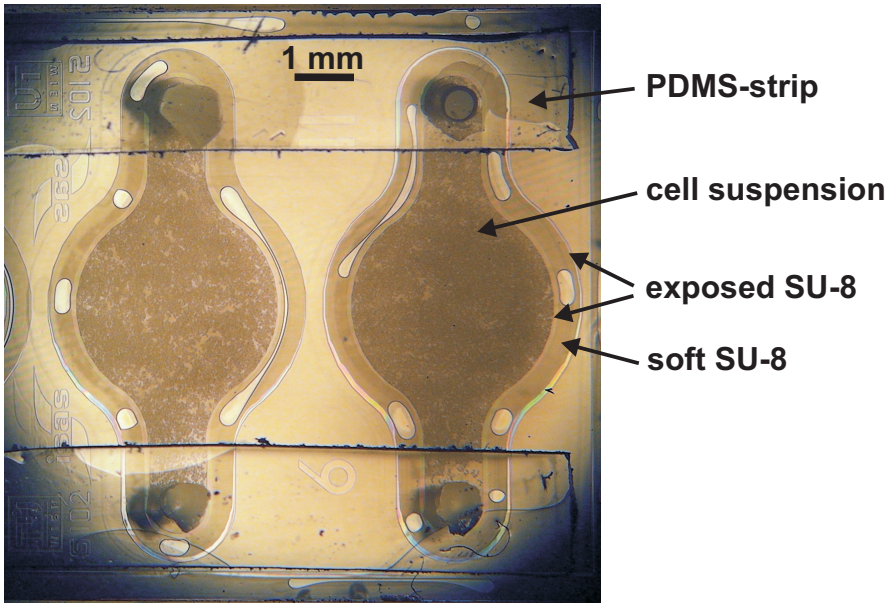

Figure 5.6: Photograph of two chambers on the chip, filled with cell suspension. The inlet and outlet holes are sealed with thin PDMS strips.

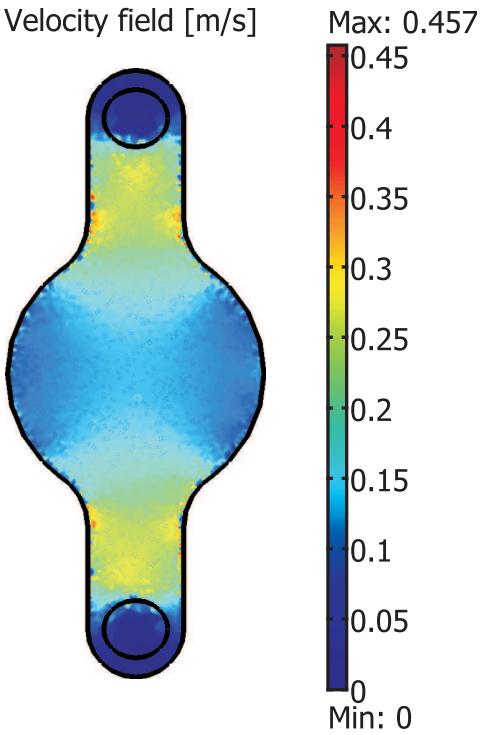

Figure 5.7: Top view of the velocity field simulated with COMSOL for a chamber height of 25 µm. Inlet hole is at the bottom, inlet velocity was 0.1 m/s. The low velocity values at inlet and outlet suggest that only little cell suspension enters the chamber volume beneath the inlet and outlet holes.

5.2 Chip fabrication

The chip has been fabricated in house in the clean room of the institute. The bonding process of the two wafers has already been described by *Svasek et al.* [45] and basically comprises the following steps: The channel on the top CaF_2 wafer is structured in such a way that the SU-8 layer comprises unexposed SU-8 enclosed by UV-exposed SU-8 side walls (see Fig. 5.8 f, g). On the bottom wafer only the exposed side walls remain (see Fig. 5.8 g). Unexposed and soft-baked SU-8 is thermoplastic and therefore the soft SU-8 from the top wafer will fill the gaps by capillary forces when heated during wafer bonding (see Fig. 5.8 h). At 150 - 200 °C unexposed SU-8 is thermally cross-linked and therefore serves as an adhesive layer between the wafers. Air bubbles which will inevitably form inside the soft SU-8 region (see Fig. 5.6) do not impair bonding efficiency. Hence, with this method insufficient wafer bonding due to a non-uniform SU-8 layer thickness is avoided. A detailed overview of the fabrication process steps as well as the used equipment and parameters are described in sections 5.2.1 - 5.2.5.

5.2.1 SU-8 deposition and patterning

In order to achieve an optimally clean surface the wafers were immersed in an ultrasound bath with 10 % RBS-50 (general purpose cleaner containing NaOH). On both CaF_2 wafers the SU-8 channel structures were fabricated as described above. Due to varying structure heights on both wafers the process parameters for SU-8 deposition differ.

Top wafer:
SU-8-50 photo resist was spun on the wafer in three consecutive steps: 200 rpm for 8 seconds, 1000 rpm for 10 seconds and 4700 rpm for 50 seconds. The resulting height was approximately 18 µm. A soft-bake (SB) step of 30 minutes at 95 °C was followed by a 50 seconds UV-exposure (a Suess MA 150 was used to align the mask on the wafer; see Fig. 5.8 a) followed by a post-exposure-bake (PEB) step for 10 minutes at 90 °C (see Fig. 5.8 b).

Bottom wafer:
SU-8-50 resist was diluted 1.5:1 with gammabutyrolactone (GBL) and spun on the wafer with 4500 rpm for 40 seconds. The resulting height was 5 µm. A SB for 20 minutes at 95°C was followed by a 20 seconds UV mask exposure and a PEB for 10 minutes at 90 °C (see Fig. 5.8 a - b). The development of SU-8 with PGMEA was done for 60 seconds in order to remove the unexposed SU-8 and obtain a height of 3.4 - 3.6 µm for the exposed SU-8 walls. Afterwards the wafer was rinsed with isopropanol.

5.2.2 Metal deposition and patterning

On the post-exposed SU-8 of only the top CaF_2 wafer a 1.2 µm thick copper (Cu) layer was vapour deposited by utilizing a Balzers BAK-550 evaporation unit (see Fig. 5.8 c). On top of the Cu layer a positive photo-resist (AZ 4512) was deposited by spinning for 40 seconds at 4000 rpm and a soft-bake step for 5 minutes at 60 °C. To finalize the photolithography an exposure step for 6 seconds and spray-development for 15 seconds with AZ 826 MIF was performed in order to remove only the exposed AZ 4512 photoresist. The Cu layer was patterned by etching in 20 % potassium

peroxydisulfate ($K_2S_2O_8$) for 3 minutes (see Fig. 5.8 d). The photo resist layer was removed with a 5 % potassium hydroxide (KOH) solution. The final development step of the SU-8 channel structure was done by immersing in propylene glycol monomethyl-ether-acetate (PGMEA) for 2.5 minutes, followed by rinsing with isopropanol (see Fig. 5.8 e). After optical inspection of the channel structure the remaining Cu was removed by immersing in a 20 % $K_2S_2O_8$ solution for 5 minutes (see Fig. 5.8 f), followed by rinsing with deionized H_2O.

5.2.3 Hole drilling

Inlets and outlets of the chips are positioned only on the bottom wafer. To prevent the wafer from contamination due to CaF_2 particles during drilling, a protective layer was deposited by spinning photoresist (AZ 4512) on top for 40 seconds at 3000 rpm and baking for 10 minutes at 60°C. 600 µm diameter inlet and outlet holes were drilled with a diamond drill, the coordinates of the inlets had been stored in the mask CAD file. After drilling the photoresist was removed with a 5 % KOH solution.

5.2.4 Wafer bonding

The top and bottom wafers were aligned, clamped to a bond tool, and inserted into an EVG 501 wafer bonder (see Fig. 5.8 g). The chamber was evacuated and the wafers were bonded by applying a force of 500 N. The temperature of the top and bottom heaters was increased to 95 °C with 3 °C/min and maintained for 30 minutes. After that, the temperature was further raised to 180 °C at the rate of 3 °C/min, then the temperature was kept stable for an additional 30 minutes (see Fig. 5.8 h). Finally the temperature was reduced to 50 °C at 1 °C/min.

5.2.5 Dicing

A DAD 3220 dicing saw with a 200 µm thick diamond blade was used to cut the bonded wafers into single chips. By placing the wafer stack with the side of the drilled inlets on an adhesive tape CaF_2 splinters were impeded to enter the channel structure via the drilled inlets.

5.2.6 Process yield

The total height of the SU-8 structures of all chips fabricated on the wafer was measured optically (FILMETRICS F20-UVX, thin film analyser) afterwards. Tab. 5.3 shows the chamber height of the chips while the corresponding chip position on the wafer is depicted in Fig. A in the appendix. As a consequence of the spin-coating process of SU-8 on CaF_2, the layer thickness varied. The resulting chamber height was larger near the centre compared to the edge of the wafer stack. Moreover, due to the fragility of CaF_2 crystals it is possible that process steps like dicing might cause breakage of CaF_2 devices. Chips too close to the edge of the wafer also could not be properly fabricated. The overall process yield was 23 / 32 chips for the first fabrication batch and 24 / 32 for the second one. With a resulting average chamber height of 21.7 µm the requirements for the IR-measurement chip were met.

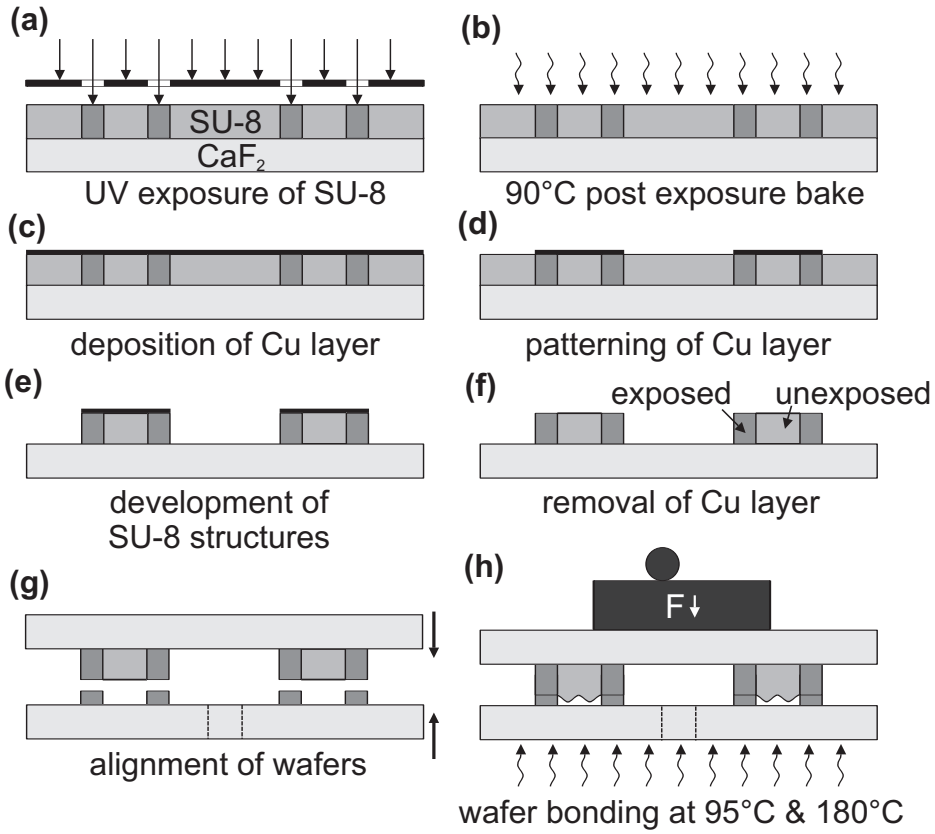

Figure 5.8: Chip fabrication steps.

Table 5.3: Total SU-8 structure height of chips fabricated on the CaF_2 wafers. The three chambers of every chip were measured optically (FILMETRICS F20-UVX, thin film analyser) and their average value is depicted. The resultant average of all chips is $21.7 \pm 0.8\,\mu m$. Chips 12 and 13 exhibit the lowest chamber height due to their position at the edge of the wafer. The position of all chips can be found in the appendix in Fig. A. Chips not listed in the table could not be fabricated due to their position on the wafer or broke during the fabrication process.

Chip number	Height [µm]
1	22.6
3	21.9
4	21.4
6	22.4
7	22.1
8	22.0
9	22.3
10	21.8
11	21.5
12	19.1
13	20.3
14	22.0
17	20.4
18	22.0
19	21.3
22	22.3
23	21.8
24	22.2
25	22.3
26	22.1
27	21.6

6 Suspended Cell Experiments

In this chapter the preparation and CH_2- and CH_3-stretch ratio measurements of cell samples suspended in PBS solution are presented. Cell samples were malignant and normal epithelial kidney cells (Caki-1 and MDCK, respectively) and human melanoma cell lines (M14, A375 and 518A2).

6.1 Sample preparation

6.1.1 Epithelial kidney cells

Epithelial kidney cells MDCK and Caki-1 were cultivated under the same conditions as described in chapter 4.1.1. They were grown attached to the bottom of culture flasks (see Fig. 6.1). In a first step the dead cells were removed from the flask by removing the culture medium. Then the attached viable cells were washed twice with PBS in order to remove the trypsin inhibitors in the Fetal Calf Serum added to the culture medium. 1 mL trypsin was added and the flask was incubated for ten minutes (MDCK) and two minutes (Caki-1), respectively, at 37 °C. After that the cells still attached to the flask bottom were released by hitting the flask several times. This suspension containing cells and trypsin was pipetted into a 15 mL test tube (see Fig. 6.2) and filled with PBS before centrifugation. The part of the centrifuged suspension with a high cell concentration was then pipetted into a 1.5 mL test tube and subsequently used for the IR absorption experiments. This tube was kept in an incubator set to 37 °C. Thus, it was possible to keep the cells alive in PBS for a few hours even without culture medium.

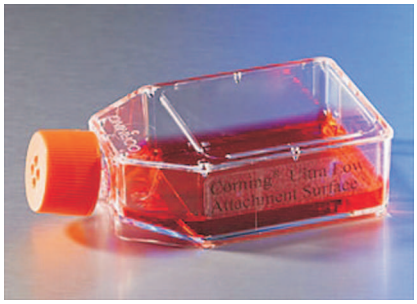

Figure 6.1: Example of a culture flask used for cell cultivation [9].

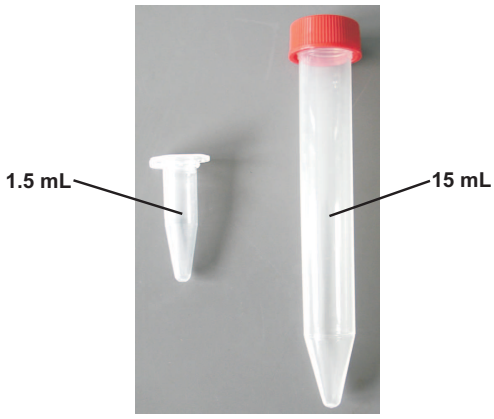

Figure 6.2: Test tubes used for cell preparation: 1.5 mL (left) and 15 mL (right).

6.1.2 Melanoma cells

The human melanoma cell lines M14, 518A2, and A375 were cultured under the same conditions as described in chapter 4.1.2 and grown in culture flasks. Cells were harvested without using trypsin but by using a cell scraper. The prepared cell samples were obtained in 1.5 mL test tubes, suspended in PBS (see Fig. 6.3). Before the measurements, clusters of cells had to be broken up into single cells or small clusters by pipetting the suspension several times in the test tube. Centrifugation was not necessary since the concentration of cells was sufficient.

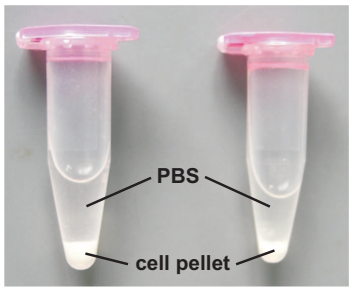

Figure 6.3: Cell samples suspended in PBS in 1.5 mL test tubes.

6.2 Measurement protocol

After switching on the equipment and the diode coolers, the LED driver currents were chosen in such a way that at the wavelength of 3.33 µm the photodiode output signal for the empty CaF_2 chip was about 4 V, which is slightly beneath the clipping voltage of the photodiode, while for the chip filled with H_2O the attenuated signal was about 0.3 - 0.4 V (see Tab. 6.1).

Table 6.1: Photodiode and LED parameters for suspended cell experiments.

	LED34	LED36	Photodiode
current:	1070 - 1080 mA	1470 - 1480 mA	-
temperature:	10.4 °C	10.7 °C	20.7 °C

6.2.1 Reference measurements

For the measurements all three chambers of the chip were filled with PBS as liquid and the inlet/outlet holes were sealed with PDMS stripes that were pressed against the chip. Then the first chamber was measured ten to twenty times and the mean value for this chamber was calculated to derive the reference signal. Afterwards PBS was removed from the first chamber by vacuum application using a SEF 520.01 vacuum pump and a rubber tube. Small droplets of PBS left in the chamber did not matter, since the subsequently measured cell suspension itself contained PBS.

6.2.2 Sample measurements

A drop of cell suspension (≈ 1 - $2\,\mu L$) was pipetted onto the inlet of the first chamber and usually entered the chamber by means of capillary forces. This could be supported by applying a light vacuum with a syringe and a rubber tube (see Fig. 6.4) in order to suck the cells through the chamber. A sufficient cell concentration in a chamber was reached when there were at least three or four spots of approximately 1.5 mm diameter (the diameter of the IR-beam) where cells were dense enough to form a confluent monolayer in the PBS buffer solution (see Figs. 6.5 and 6.6). Optical inspection was done with a Zeiss Stemi SV11 optical microscope. Again the inlet holes were sealed with PDMS. Three to five spots were measured, depending on the density and distribution of cells. Per spot seven to ten measurements were conducted.

After measuring the first chamber the same procedure (reference measurements, filling with cell suspension and sample measurements) was applied to the other two chambers. Since the height of the three chambers on a single chip varied slightly (≈ 0.5 - $1\,\mu m$), the reference and sample measurements had to take place in the same chamber and not in two adjacent ones. An adequate number of measurements of all three chambers, that is about ten spots, could usually be achieved within two hours. Provided that enough sample was left, a second sample batch could be measured either in a new chip or, after cleaning, in the same chip.

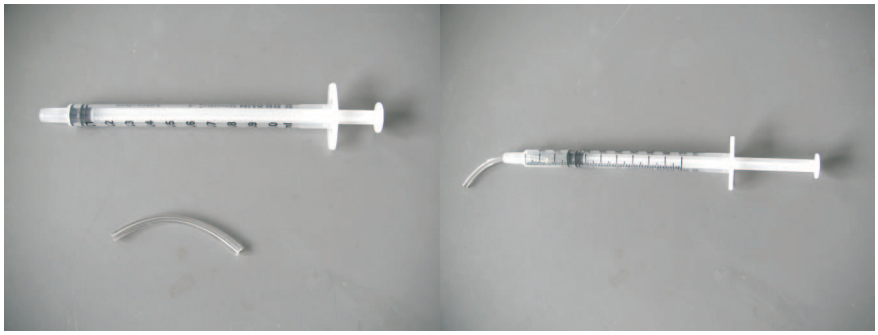

Figure 6.4: A 1 mL syringe and a short piece of flexible rubber tube (left) that could be combined (right) in order to apply a very small vacuum.

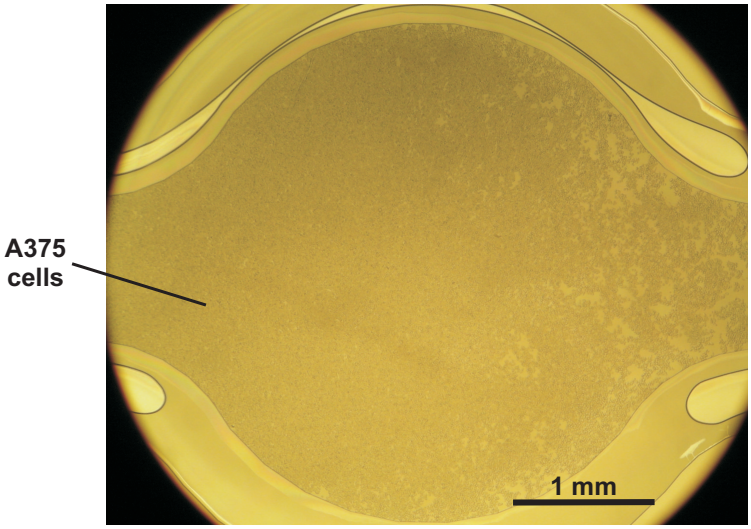

Figure 6.5: Photograph of a chamber filled with A375 cell suspension. Cell concentration is sufficiently high at four different measurement spots.

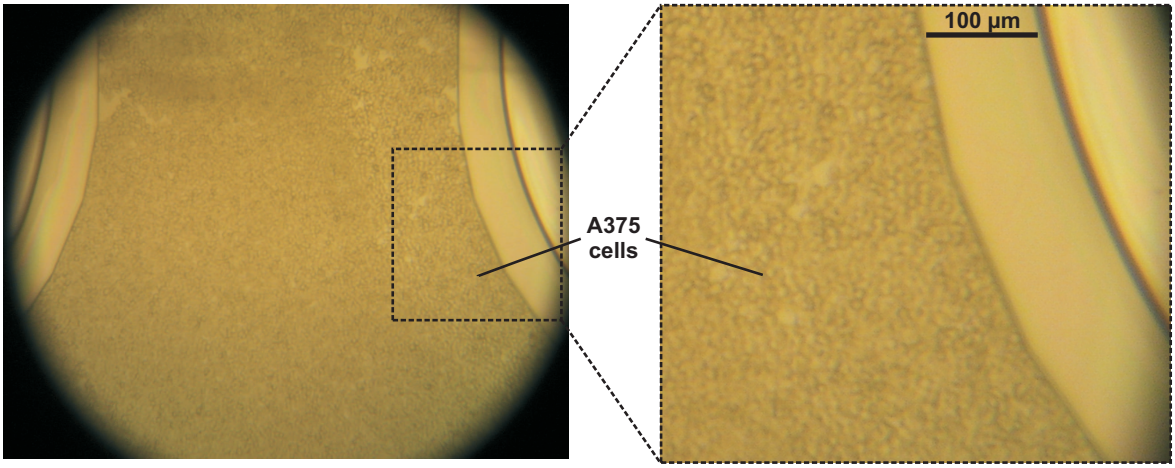

Figure 6.6: Detailed view of A375 cell suspension in the region close to the inlet hole.

6.2.3 Cleaning

Chambers that contained cell samples were flushed with DanKlorix using a 10 mL syringe with an attached rubber tube that was pressed against the inlet. DanKlorix is an alkaline commercial household cleaner and disinfectant containing sodium carbonate and sodium hypochlorite with the ability to dissolve biological cells. This way the majority of the cells could be removed instantly, while any remaining cells were slowly dissolved in the chambers filled with DanKlorix. After 20 - 30 minutes the chambers were flushed with water several times. The outer surfaces of the chip were cleaned with water and isopropanol or ethanol to remove stains or fingerprints.

6.3 Results and discussion

6.3.1 Epithelial kidney cells

Two MDCK and three Caki-1 cell samples were prepared and measured in order to compare their CH_2- and CH_3-stretch ratios. MDCK and Caki-1 samples were measured within five weeks and two months, respectively. The number of spots measured per sample was about five, depending on the cell concentration. The following figures and tables show the average value and standard deviation of all spots recorded for one sample. Spots with a standard deviation higher than 0.05 were discarded.

As depicted in Fig. 6.7 and Tab. 6.2 the CH_2-stretch ratio is higher for PBS suspended Caki-1 compared to MDCK (average of all samples: 0.48 and 0.44). Fig. 6.8 and Tab. 6.3 show the same behaviour for Caki-1 and MDCK with respect to the CH_3-stretch ratio (average values: 0.65 and 0.57).

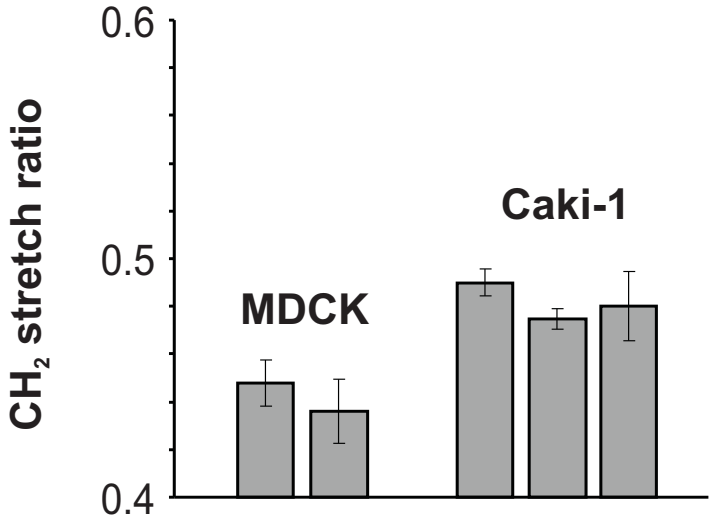

Figure 6.7: CH_2-stretch ratio of MDCK and Caki-1 cell lines. The grey bars indicate the average ratio of all spots measured per sample, the error bars indicate the standard deviation.

Table 6.2: Average values and standard deviation of the CH_2-stretch ratio for epithelial kidney cell lines MDCK and Caki-1.

	CH_2-stretch ratio
MDCK sample 1	0.45 ± 0.01
MDCK sample 2	0.44 ± 0.01
Caki-1 sample 1	0.49 ± 0.01
Caki-1 sample 2	0.48 ± 0.01
Caki-1 sample 3	0.48 ± 0.02

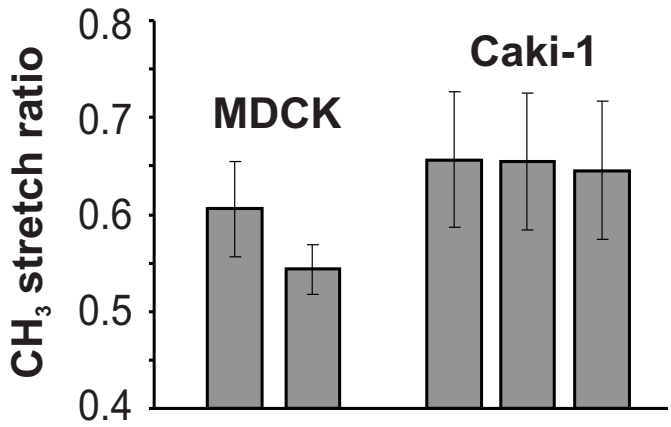

Figure 6.8: CH_3-stretch ratio of MDCK and Caki-1 cell lines. The grey bars indicate the average ratio of all spots measured per sample, the error bars indicate the standard deviation.

Table 6.3: Average values and standard deviation of the CH_3-stretch ratio for epithelial kidney cell lines MDCK and Caki-1.

	CH_3-stretch ratio
MDCK sample 1	0.60 ± 0.05
MDCK sample 2	0.54 ± 0.03
Caki-1 sample 1	0.66 ± 0.07
Caki-1 sample 2	0.66 ± 0.07
Caki-1 sample 3	0.65 ± 0.07

6.3.2 Melanoma cells

Suspended melanoma cell lines M14, A375, and 518A2 were measured in order to compare their CH_2- and CH_3-stretch ratios. Two to three samples per cell line were obtained and all samples were measured within one month. The number of spots measured per sample was about five, depending on the cell concentration. The following figures and tables show the average value and standard deviation of all spots recorded for one sample.

The CH_2-stretch ratios are depicted in Fig. 6.9 and Tab. 6.4. Average values of all samples recorded were 0.42 (M14), 0.45 (A375), and 0.48 (518A2). The CH_3-stretch ratio shows a similar behaviour as can be seen in Fig. 6.10 and Tab. 6.5, resulting in average values of 0.53 (M14), 0.57 (A375), and 0.64 (518A2).

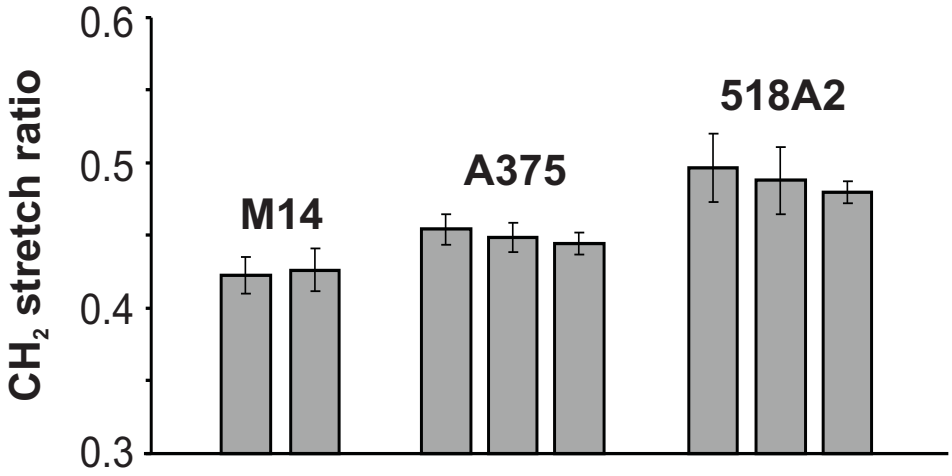

Figure 6.9: CH_2-stretch ratio of melanoma cell lines M14, A375, and 518A2. The grey bars indicate the average ratio of all spots measured per sample, the error bars indicate the standard deviation.

Table 6.4: Average values and standard deviation of the CH_2-stretch ratio for melanoma cell lines M14, A375, and 518A2.

	CH_2-stretch ratio
M14 sample 1	0.42 ± 0.01
M14 sample 2	0.43 ± 0.01
A375 sample 1	0.45 ± 0.01
A375 sample 2	0.45 ± 0.01
A375 sample 3	0.45 ± 0.01
518A2 sample 1	0.50 ± 0.02
518A2 sample 2	0.49 ± 0.02
518A2 sample 3	0.48 ± 0.01

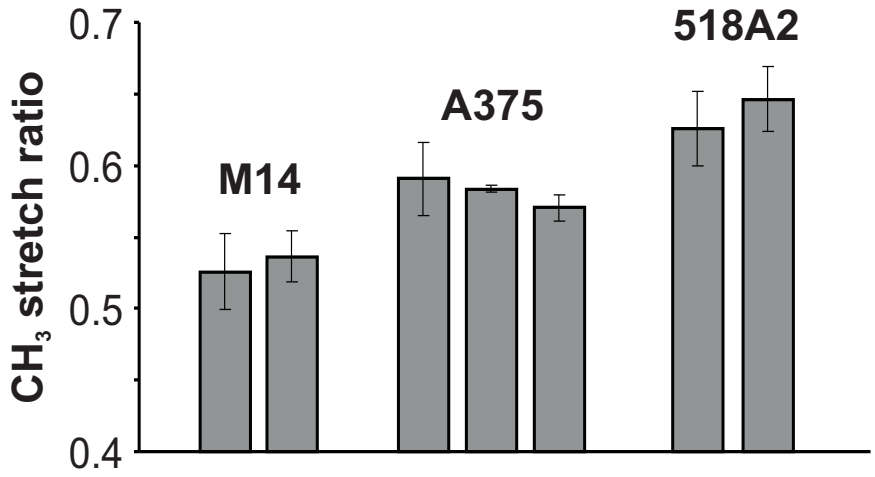

Figure 6.10: CH_3-stretch ratio of melanoma cell lines M14, A375, and 518A2. The grey bars indicate the average ratio of all spots measured per sample, the error bars indicate the standard deviation.

Table 6.5: Average values and standard deviation of the CH_3-stretch ratio for melanoma cell lines M14, A375, and 518A2.

	CH_3-stretch ratio
M14 sample 1	0.53 ± 0.03
M14 sample 2	0.54 ± 0.02
A375 sample 1	0.59 ± 0.03
A375 sample 2	0.58 ± 0.03
A375 sample 3	0.57 ± 0.01
518A2 sample 1	0.63 ± 0.02
518A2 sample 2	0.65 ± 0.02

7 Conclusions and Outlook

In this thesis a cost-effective sensor system for IR absorption measurements of biological cell samples was presented. The sensor system measures the amount of absorbed IR light only at distinct wavelengths that are characteristic for CH_2- and CH_3-stretch vibrations. In a literature study we compared the IR absorbance spectra of normal and tumour cells between the wavelengths 3.3 - 3.7 µm and found the CH_2-symmetric / CH_2-antisymmetric stretch ratio to be significantly increased for tumour cells. This was supported by measurements conducted on epithelial kidney cell lines with a conventional FTIR spectrometer. Also, changes of the CH_3-symmetric and CH_3-antisymmetric stretch absorbance were evident.

With the sensor system the functional absorptance values for symmetric and antisymmetric CH_2- and CH_3-stretches were determined and subsequently used to derive the stretch ratios. The CH_2- and CH_3-stretch ratios of normal and tumour epithelial kidney cell lines (MDCK and Caki-1) as well as three different melanoma cell lines (M14, A375, and 518A2) were compared. Measurements were done with dried cells as well as cells suspended in PBS. Therefore, a microfluidic chip made of IR-transparent CaF_2 comprising SU-8 microchambers was designed and fabricated.

7.1 Dried cells

7.1.1 Epithelial kidney cells

Our measurements showed that dried MDCK have an average CH_2-stretch ratio of 0.47 compared to 0.71 for Caki-1. This confirmed previously own published research results that found a higher CH_2-stretch ratio for tumour cells compared to healthy cells. The average CH_3-stretch ratios were 0.63 (MDCK) and 1.22 (Caki-1). Thus, both CH_2- and CH_3-stretch ratio have the potential for cell type discrimination.

7.1.2 Melanoma cells

Dried melanoma cell samples included M14 and A375 cell lines. The CH_2-stretch ratio has been compared for untreated cells and cisplatin-treated cells. Average CH_2-stretch ratio of untreated M14 cells was 0.58, while for cisplatin incubated M14 it was 0.44. For A375 it was 0.74 (untreated) compared to 0.51 (treated). These results suggest that the sensing method can also be used to determine the effectiveness of chemotherapy drugs on tumour cells.

7.2 Suspended cells

7.2.1 Epithelial kidney cells

Measurements of suspended MDCK and Caki-1 cells yielded CH_2-stretch ratios of 0.44 and 0.48, while the CH_3-stretch ratios were 0.57 and 0.65. Also, measurement uncertainties were higher for suspended cell measurements compared to dried cell measurements. The difference between the ratios of normal and tumour cells is smaller than for dried cells, e.g. CH_2-stretch ratio difference for dried and suspended cell experiments, respectively, was 0.24 compared to 0.04, but still larger than the standard deviation (≈ 0.01).

7.2.2 Melanoma cells

Suspended melanoma cells included M14, A375, and 518A2 cell lines. The average CH_2-stretch ratios were 0.42 (M14), 0.45 (A375), and 0.48 (518A2), respectively. Again the trend for the CH_3-stretch ratios is the same as for the CH_2-stretch ratios: 0.53 (M14), 0.57 (A375), and 0.64 (518A2). A distinction of the three different melanoma cell lines is thus possible by comparing their CH_2- or CH_3-stretch ratios. Similar to epithelial kidney cells, the difference in resulting CH_2-stretch ratios is higher for dried cells compared to cells in suspension. The differences for M14 and A375 are 0.16 (dried) and 0.03 (suspended), respectively, with a standard deviation of ≈ 0.01.

7.3 CH_2- and CH_3-stretch ratio

It can be stated that both CH_2- and CH_3-stretch ratios can be utilized to differentiate between normal and tumour cells of a certain origin as well as between different melanoma cell lines. The significance of the CH_2-stretch ratios is higher due to the more pronounced absorbance peaks and the amount of lipid CH_2 molecules in cell membranes compared to CH_3.

Measurements of suspended cells have the advantage of shorter sample preparation times compared to dried cells, since they can be prepared within half an hour, and also allow for the measurements of viable cells.

The measurement results of cells suspended in PBS were in accord with those from dried cell measurements, although the distinction was not as clear as for dried cells. Despite the larger standard deviations compared to dried cell measurements, the results were comparable and reproducible for each cell line. Influences on the standard deviation might have been the reduced signal-to-noise level of the PD output voltage due to the high absorbance of water or a variation of cell concentration in the measurement chambers.

Measurements of cell samples with different cell passage number and also measurements with different chips, hence varying chamber heights, yielded similar results, which confirmed the effectiveness of the proposed method.

7.4 Outlook

Without a doubt, a higher signal-to-noise level would improve suspended cell measurements. As a consequence, either the chamber height and hence the thickness of the water layer has to be reduced or IR light intensity has to be increased. The first option is not feasible, because of the cell size. Presently, the cell size is already restricted due to a chamber height of about 20 µm. Using a suspension liquid that is absorbing less IR radiation in the 3.3 - 3.7 µm range such as D_2O would be equal to reducing chamber height, but has proven to be more difficult, since is did not behave stable in time. However, further investigation of D_2O and different mixture ratios with H_2O is indicated. Thus, a challenging option would be to use IR sources and corresponding drivers that provide a higher IR light intensity or mid-IR lasers like QCLs (quantum cascade lasers).

Additionally, an optimisation of the pulse shape and duration, as well as the number of sample spots could be investigated in order to achieve measurement results with a lower standard deviation. A trade-off between sufficiently low standard deviation and short acquisition time would have to be found. Automated filter wheels that are controlled by a MATLAB script could replace the manual changing of filter wheels to the next position. But except for minimal time savings this measure would not improve the measurement process.

Appendix

MATLAB code

measure.m

```
function r = measure(Filename, AInputChannel, Comment, SampleTime, MaxUsed,
    no_of_measurements)
clc;
%Start daq with NI USB-6251
r.SampleTime          = SampleTime;
r.MaxUsed             = MaxUsed;
r.no_of_measurements  = no_of_measurements;
r.Filename            = Filename;
r.AInputChannel       = AInputChannel;
r.Comment             = Comment;

disp (r.Filename);
%Run basepoint measurement
bp(r.Filename, r.AInputChannel, r.Comment, r.SampleTime, r.MaxUsed,
    r.no_of_measurements);
disp ' ';
disp('Change the filters to 3415 & 3505nm and press a key')
w = waitforbuttonpress;
if w == 0
    disp('Button clicked')
else
    disp('Key pressed')
end

%Run functional group measurement
fg_ch2(r.Filename, r.AInputChannel, r.Comment, r.SampleTime, r.MaxUsed,
    r.no_of_measurements);


disp ' ';
disp('Change the filters to 3385 & 3485nm and press a key')
w = waitforbuttonpress;
if w == 0
    disp('Button clicked')
else
    disp('Key pressed')
```

```
end

%Run functional group measurement
fg_ch3(r.Filename, r.AInputChannel, r.Comment, r.SampleTime, r.MaxUsed,
    r.no_of_measurements);



% Read out the files that were saved before in the led34 and led36 routines and
    delete temporary files

f=['3335', '3385', '3415', '3485', '3505', '3565'];
v=[0,0,0,0,0,0];

for i=0:5

file=sprintf('%s %s%s%s%s%s', Filename, f(4*i+1),f(4*i+2),f(4*i+3),
    f(4*i+4),'.mat'); % generate filename
load(file);

v(i+1)=value; % read out and store measured value
delete(file);

end


% Save all six measured values in a new file together with corresponding
% filter names and put current clock in the filename
c=fix(clock);
FilenameClock = sprintf('%s RESULT %i-%i-%i %ih%im%is.mat',Filename,
    c(3),c(2),c(1),c(4),c(5),c(6));
x=[3335, 3385, 3415, 3485, 3505, 3565];

save(FilenameClock, 'x', 'v')


% Plot the measured values
stem(x,v);


% Return measured values to the MATLAB user interface
r.Result=v;
```

bp.m

```
function q = bp(Filename, AInputChannel, Comment, SampleTime, MaxUsed,
    no_of_measurements)

%Start daq with NI USB-6251
q.SampleTime          = SampleTime;
q.maxused             = MaxUsed;
q.no_of_measurements  = no_of_measurements;
q.Filename            = Filename;
q.AInputChannel       = AInputChannel;
q.Comment             = Comment;

disp 'BASEPOINTS:';
%Run basepoint measurement
```

```
p=led34(q.Filename, '3335', q.AInputChannel, q.Comment, q.SampleTime, q.maxused,
    q.no_of_measurements);
q.v34=p.AverageMax3;

p=led36(q.Filename, '3565', q.AInputChannel, q.Comment, q.SampleTime, q.maxused,
    q.no_of_measurements);
q.v36=p.AverageMax3;
```

fg_ch2.m

```
function q = fg(Filename, AInputChannel, Comment, SampleTime, MaxUsed,
    no_of_measurements)

%Start daq with NI USB-6251
q.SampleTime          = SampleTime;
q.maxused             = MaxUsed;
q.no_of_measurements  = no_of_measurements;
q.Filename            = Filename;
q.AInputChannel       = AInputChannel;
q.Comment             = Comment;

disp ' ';
disp 'FUNCTIONAL GROUPS CH_2:';
%Run basepoint measurement
led34(q.Filename, '3415', q.AInputChannel, q.Comment, q.SampleTime, q.maxused,
    q.no_of_measurements);

led36(q.Filename, '3505', q.AInputChannel, q.Comment, q.SampleTime, q.maxused,
    q.no_of_measurements);
```

fg_ch3.m

```
function q = fg_ch3(Filename, AInputChannel, Comment, SampleTime, MaxUsed,
    no_of_measurements)

%Start daq with NI USB-6251
q.SampleTime          = SampleTime;
q.maxused             = MaxUsed;
q.no_of_measurements  = no_of_measurements;
q.Filename            = Filename;
q.AInputChannel       = AInputChannel;
q.Comment             = Comment;

disp ' ';
disp 'FUNCTIONAL GROUPS CH_3:';
%Run basepoint measurement
led34(q.Filename, '3385', q.AInputChannel, q.Comment, q.SampleTime, q.maxused,
    q.no_of_measurements);

led36(q.Filename, '3485', q.AInputChannel, q.Comment, q.SampleTime, q.maxused,
    q.no_of_measurements);
```

led34.m

```
function p = led34(Filename, Filter, AInputChannel, Comment, SampleTime, MaxUsed,
    no_of_measurements)

%Start daq with NI USB-6251
p.SampleTime          = SampleTime;
p.TriggerTimeout      = 2; %If there is no trigger signal after 2 seconds time out
p.maxused             = MaxUsed;
p.no_of_measurements  = no_of_measurements;
p.Filename            = Filename;
p.Filtername          = Filter;
p.SampleRate          = 1250000; %Maximum samplerate for NI USB-6251
p.InputRange          = [-5 5]; %Amplifier output 0-4V
p.AInputChannel       = AInputChannel;
p.Comment             = Comment;

ai = analoginput ('nidaq','Dev1');
ch = addchannel(ai,p.AInputChannel,{'PD'});
ch.InputRange = p.InputRange;
ai.SampleRate = p.SampleRate;
ai.SamplesPerTrigger = ai.SampleRate*p.SampleTime;

%Trigger parameters
set(ai,'TriggerType','HwDigital');
set(ai,'HwDigitalTriggerSource','PFI0'); %Specify dio port
set(ai,'TriggerCondition','PositiveEdge');

j=1;
timeout = false;
tic;

for i=1:p.no_of_measurements
        start(ai);
    try
       wait(ai,p.TriggerTimeout);
    catch
       disp('Trigger Timeout');
       timeout = true;
    end
     if timeout == false
         p.data(:,j) = getdata(ai); %read data
%         disp (sprintf('Sample %i of %i',i,p.no_of_measurements));
         stop(ai);
         j=j+1;
     else
        stop(ai);
        timeout = false;
    end;
end
p.TotalTime = toc; %time needed for the for loop
p.no_of_timeouts = p.no_of_measurements - size(p.data,2);
disp(sprintf('Total time for %i measurements: %i seconds. No. Timeouts: %i',
    p.no_of_measurements, round(p.TotalTime), p.no_of_timeouts))
stop(ai);
delete(ai);    %delete objects

%Extraction of # maximums per no_of_measurements
```

```
dataset=p.data;

[C,I]=max(dataset);
n=1;
for n=1:size(C,2)    %no of measurements recorded
    dataset(I(n),n)=0;  %erase the max value per column with 0
    n=n+1;
end;

k=1;
for k=1:p.maxused
    [C,I]=max(dataset);  %create C, max values per column, I indices of the max
        value per column
    p.newdata(k,:)=C;    %create data set with max values
    k=k+1;

    l=1;
    for l=1:size(C,2)    %no of measurements recorded
        dataset(I(l),l)=0;  %erase the max value per column with 0
        l=l+1;
    end;
end

m=1;
for m=1:size(C,2)
    p.AverageMaxPerMeasurement(:,m)=mean(p.newdata(:,m)); %calculate the average of
        the # highest values per measurement
end

p.AverageMax = mean(p.AverageMaxPerMeasurement); %average the maximums of all
    measurements
p.SamplesPerMeasurement = size(p.data,1);
p.stdev = std(p.AverageMaxPerMeasurement);


p.timescale=linspace(0,p.SampleTime, p.SampleRate*p.SampleTime); %seconds
p.difminmax=((p.newdata(1,:))-(p.newdata(p.maxused,:)));

%Test and remove measurements which have a higher max-min (of the four second
    highest values) value than 0.1 V
r=1;
s=1;
for r=1:size(p.difminmax,2)
    if (p.difminmax(1,r))<0.1  %every measurement with less than 0.1 V difference
        between max and min is stored in a new dataset
        p.newdata2(:,s)=p.newdata(:,r);
        p.data2(:,s)=p.data(:,r);
        s=s+1;
    else
    end;
end
t=1;
for t=1:size(p.newdata2,2)
    p.AverageMaxPerMeasurement2(:,t)=mean(p.newdata2(:,t));
end
p.AverageMax2=mean(p.AverageMaxPerMeasurement2);
p.stdev2=std(p.AverageMaxPerMeasurement2);

% Offset value calc per measurement
```

```
if p.SamplesPerMeasurement>20
   dataset2=p.data2;
    q=20;
    for q=20:p.SamplesPerMeasurement
        p.newdata3(q-19,:)=dataset2(q,:);
    end
    y=1;
    for y=1:size(p.newdata3,2)
        p.AverageMinPerMeasurement(:,y)=mean(p.newdata3(:,y));
    end
    % Value - Offset calc
    p.OffsetAdj=p.AverageMaxPerMeasurement2-p.AverageMinPerMeasurement;
    p.AverageMax3=mean(p.OffsetAdj);
    p.stdev3=std(p.OffsetAdj);
else
    disp(sprintf('no Offset calculated!'))
end


%Filename to save data
c=fix(clock);
p.FilenameWithClock = sprintf('%s %s %i-%i-%i %ih%im%is.mat',p.Filename,
    p.Filtername ,c(3),c(2),c(1),c(4),c(5),c(6));
save(p.FilenameWithClock, 'p');


%save average value and filter name in a temporary file which is read out later
value=p.AverageMax3;
filter=p.Filtername;
p.FileFilter = sprintf('%s %s.mat',p.Filename, p.Filtername);
save(p.FileFilter, 'value', 'filter');
%changes end

disp(sprintf('AverageMax3 filter %s= %0.4g V. stdev3 = %0.4g V', p.Filtername,
    p.AverageMax3, p.stdev3));
disp(sprintf('Saved data to %s',p.FilenameWithClock));
disp ' ';
```

led36.m

```
function p = led36(Filename, Filter, AInputChannel, Comment, SampleTime, MaxUsed,
    no_of_measurements)
% p = led36(Filename, Filter, AInputChannel,Comment,SampleTime,MaxUsed,
    no_of_measurements)

%Start daq with NI USB-6251
p.SampleTime          = SampleTime;
p.TriggerTimeout      = 2; %If there is no trigger signal after 2 seconds time out
p.maxused             = MaxUsed;
p.no_of_measurements  = no_of_measurements;
p.Filename            = Filename;
p.Filtername          = Filter;
p.SampleRate          = 1250000; %Maximum samplerate for NI USB-6251
p.InputRange          = [-5 5]; %Amplifier output 0-4V
p.AInputChannel       = AInputChannel;
p.Comment             = Comment;

ai = analoginput ('nidaq','Dev1');
ch = addchannel(ai,p.AInputChannel,{'PD'});
ch.InputRange = p.InputRange;
ai.SampleRate = p.SampleRate;
ai.SamplesPerTrigger = ai.SampleRate*p.SampleTime;

%Trigger parameters
set(ai,'TriggerType','HwDigital');
set(ai,'HwDigitalTriggerSource','PFI1'); %Specify dio port
set(ai,'TriggerCondition','PositiveEdge');

j=1;
timeout = false;
tic;

for i=1:p.no_of_measurements
        start(ai);
    try
       wait(ai,p.TriggerTimeout);
    catch
       disp('Trigger Timeout');
       timeout = true;
    end
     if timeout == false
         p.data(:,j) = getdata(ai); %read data
%         disp (sprintf('Sample %i of %i',i,p.no_of_measurements));
         stop(ai);
         j=j+1;
     else
        stop(ai);
        timeout = false;
    end;
end
p.TotalTime = toc; %time needed for the for loop
p.no_of_timeouts = p.no_of_measurements - size(p.data,2);
disp(sprintf('Total time for %i measurements: %i seconds. No. Timeouts: %i',
    p.no_of_measurements, round(p.TotalTime), p.no_of_timeouts))
stop(ai);
delete(ai);    %delete objects
```

```
%Extraction of # maximums per no_of_measurements
dataset=p.data;

[C,I]=max(dataset);
n=1;
for n=1:size(C,2)    %no of measurements recorded
    dataset(I(n),n)=0;  %erase the max value per column with 0
    n=n+1;
end;

k=1;
for k=1:p.maxused
    [C,I]=max(dataset);  %create C, max values per column, I indices of the max
        value per column
    p.newdata(k,:)=C;    %create data set with max values
    k=k+1;

    l=1;
    for l=1:size(C,2)    %no of measurements recorded
        dataset(I(l),l)=0;  %erase the max value per column with 0
        l=l+1;
    end;
end

m=1;
for m=1:size(C,2)
    p.AverageMaxPerMeasurement(:,m)=mean(p.newdata(:,m)); %calculate the average of
        the # highest values per measurement
end

p.AverageMax = mean(p.AverageMaxPerMeasurement); %average the maximums of all
    measurements
p.SamplesPerMeasurement = size(p.data,1);
p.stdev = std(p.AverageMaxPerMeasurement);

p.timescale=linspace(0,p.SampleTime, p.SampleRate*p.SampleTime); %seconds
p.difminmax=((p.newdata(1,:))-(p.newdata(p.maxused,:)));

%Test and remove measurements which have a higher max-min (of the four second
    highest values) value than 0.1 V
r=1;
s=1;
for r=1:size(p.difminmax,2)
    if (p.difminmax(1,r))<0.1  %every measurement with less than 0.1 V difference
        between max and min is stored in a new dataset
        p.newdata2(:,s)=p.newdata(:,r);
        p.data2(:,s)=p.data(:,r);
        s=s+1;
    else
    end;
end
t=1;
for t=1:size(p.newdata2,2)
    p.AverageMaxPerMeasurement2(:,t)=mean(p.newdata2(:,t));
end
p.AverageMax2=mean(p.AverageMaxPerMeasurement2);
p.stdev2=std(p.AverageMaxPerMeasurement2);
```

```
% Offset value calc per measurement

if p.SamplesPerMeasurement>20
   dataset2=p.data2;
    q=20;
    for q=20:p.SamplesPerMeasurement
        p.newdata3(q-19,:)=dataset2(q,:);
    end
    y=1;
    for y=1:size(p.newdata3,2)
        p.AverageMinPerMeasurement(:,y)=mean(p.newdata3(:,y));
    end
    % Value - Offset calc
    p.OffsetAdj=p.AverageMaxPerMeasurement2-p.AverageMinPerMeasurement;
    p.AverageMax3=mean(p.OffsetAdj);
    p.stdev3=std(p.OffsetAdj);
else
    disp(sprintf('no Offset calculated!'))
end


%Filename to save data
c=fix(clock);
p.FilenameWithClock = sprintf('%s %s %i-%i-%i %ih%im%is.mat',p.Filename,
    p.Filtername ,c(3),c(2),c(1),c(4),c(5),c(6));
save(p.FilenameWithClock, 'p');


%save average value and filter name in a temporary file which is read out later
value=p.AverageMax3;
filter=p.Filtername;
p.FileFilter = sprintf('%s %s.mat',p.Filename, p.Filtername);
save(p.FileFilter, 'value', 'filter');
%changes end

disp(sprintf('AverageMax3 filter %s= %0.4g V. stdev3 = %0.4g V', p.Filtername,
    p.AverageMax3, p.stdev3));
disp(sprintf('Saved data to %s',p.FilenameWithClock));
disp ' ';
```

plot_voltage.m

```
function plot_voltage(R)
% pass a matrix with measurement results for each of the six wavelengths

% vector with filter wavelengths
x=[3335; 3385; 3415; 3485; 3505; 3565];

% generate an empty figure at a proper place on the screen
close all
scrsz = get(0,'ScreenSize');
figure('Position',[scrsz(3)/2 -scrsz(4)/15 scrsz(3)/2 scrsz(4)])

for i=1:6
    % plot each wavelength in a different subplot
    subplot(3,2,i)

    % plot all measurement values for a certain wavelength in one plot
    plot(R(:,i),'-x')

    % title the subplot with the filter name
    title(x(i))

    % print mean value and standard deviation for each subplot
    xlabel([num2str(mean(R(:,i))), ' +/- ', num2str(std(R(:,i)))])
end
```

ratio.m

```
function [v,CH]=ratio(a,b)
% pass the measured sample & reference values
% and return functional absorbance values & ratios

% vector with filter wavelengths
x=[3335; 3385; 3415; 3485; 3505; 3565];

aa=a';
s=size(aa);
for i=1:s(2)
abs(:,i)=100-aa(:,i)./b'*100; % calculate absorptance
end

% calculate baseline corrected absorbtance values
% for CH2 and CH3 wavelengths

%3385
v3385=abs(2,:)-(abs(1,:)+(x(2)-x(1))/(x(6)-x(1)).*(abs(6,:)-abs(1,:)));

%3415
v3415=abs(3,:)-(abs(1,:)+(x(3)-x(1))/(x(6)-x(1)).*(abs(6,:)-abs(1,:)));

%3485
v3485=abs(4,:)-(abs(1,:)+(x(4)-x(1))/(x(6)-x(1)).*(abs(6,:)-abs(1,:)));

%3505
v3505=abs(5,:)-(abs(1,:)+(x(5)-x(1))/(x(6)-x(1)).*(abs(6,:)-abs(1,:)));
```

```
% calcualte ratios
rat=v3505./v3415;       % CH2
rat_sym=v3485./v3385;   % CH3
rat_asym=v3385./v3415;  % antisymmetric


% vector with functional absorbance values
v=[v3385; v3415; v3485; v3505]';
% vector with ratios
CH=[rat;rat_asym;rat_sym];


% plot ratios
scrsz = get(0,'ScreenSize');
figure('Position',[scrsz(3)/20 scrsz(4)/2-scrsz(4)/10 scrsz(3)-scrsz(3)/10
    scrsz(4)/2])

subplot(1,3,1)
bar(v3505./v3415)
title(['CH2sym/CH2asym - average ratio = ', num2str(mean(v3505./v3415)),
                                '  std = ', num2str(std(mean(v3505./v3415))) ])
xlabel('measurement')
ylabel('3505/3415')


subplot(1,3,3)
bar(v3485./v3385)
title(['ratio CH3sym/CH3asym - average ratio = ', num2str(mean(v3485./v3385)),
                                    '  std = ', num2str(std(v3485./v3385)) ])
xlabel('measurement')
ylabel('3485/3385')


subplot(1,3,2)
bar(v3385./v3415)
title(['CH3asym/CH2asym - average ratio = ', num2str(mean(v3385./v3415)),
                                '  std = ', num2str(std(v3385./v3415)) ])
xlabel('measurement')
ylabel('3385/3415')
```

Device Masks

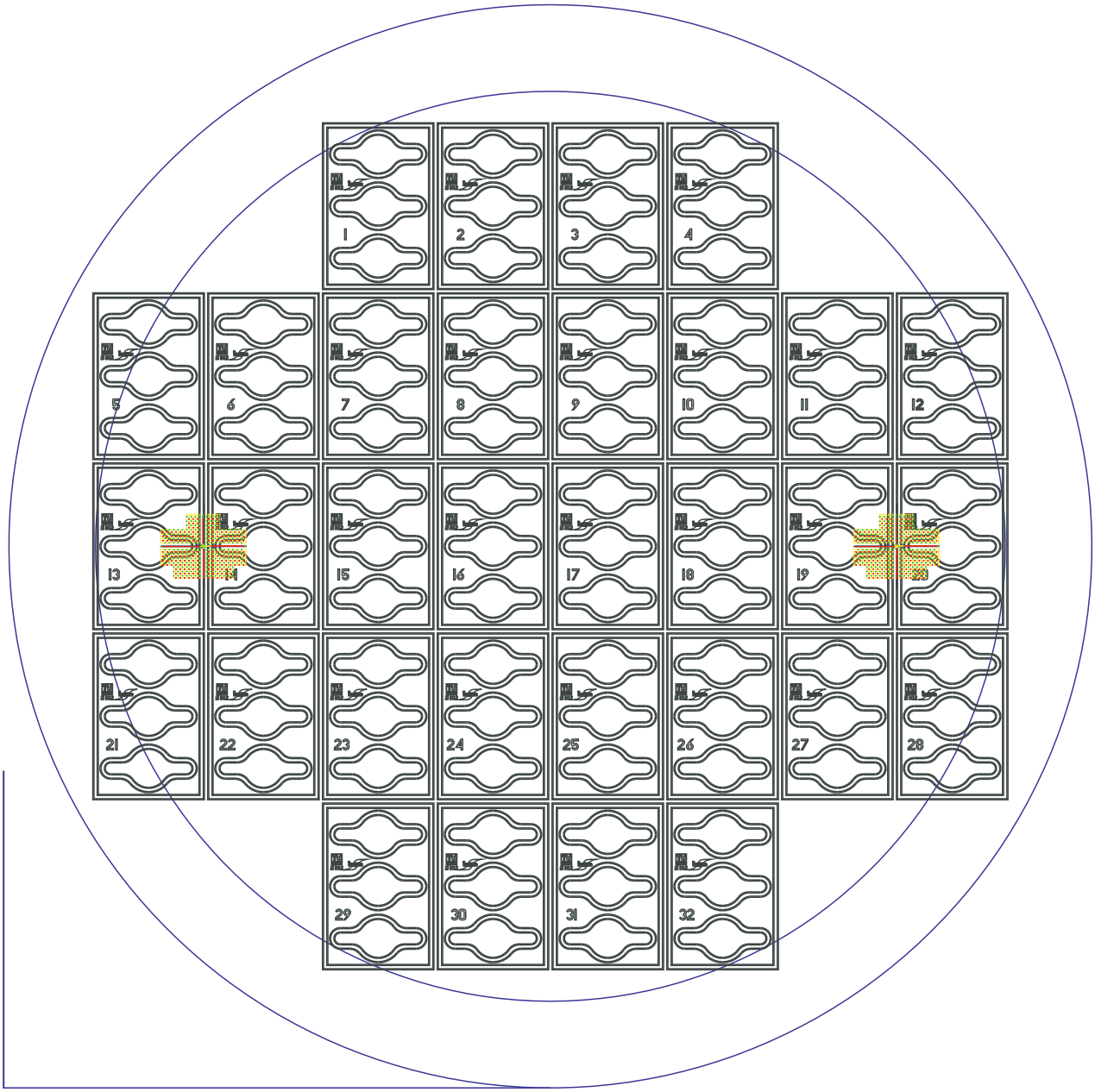

Figure A: Mask for SU-8 structuring. The mask layout is symmetrical along the vertical axis, since on the bottom and top wafer of the wafer stack the same SU-8 structures were fabricated.

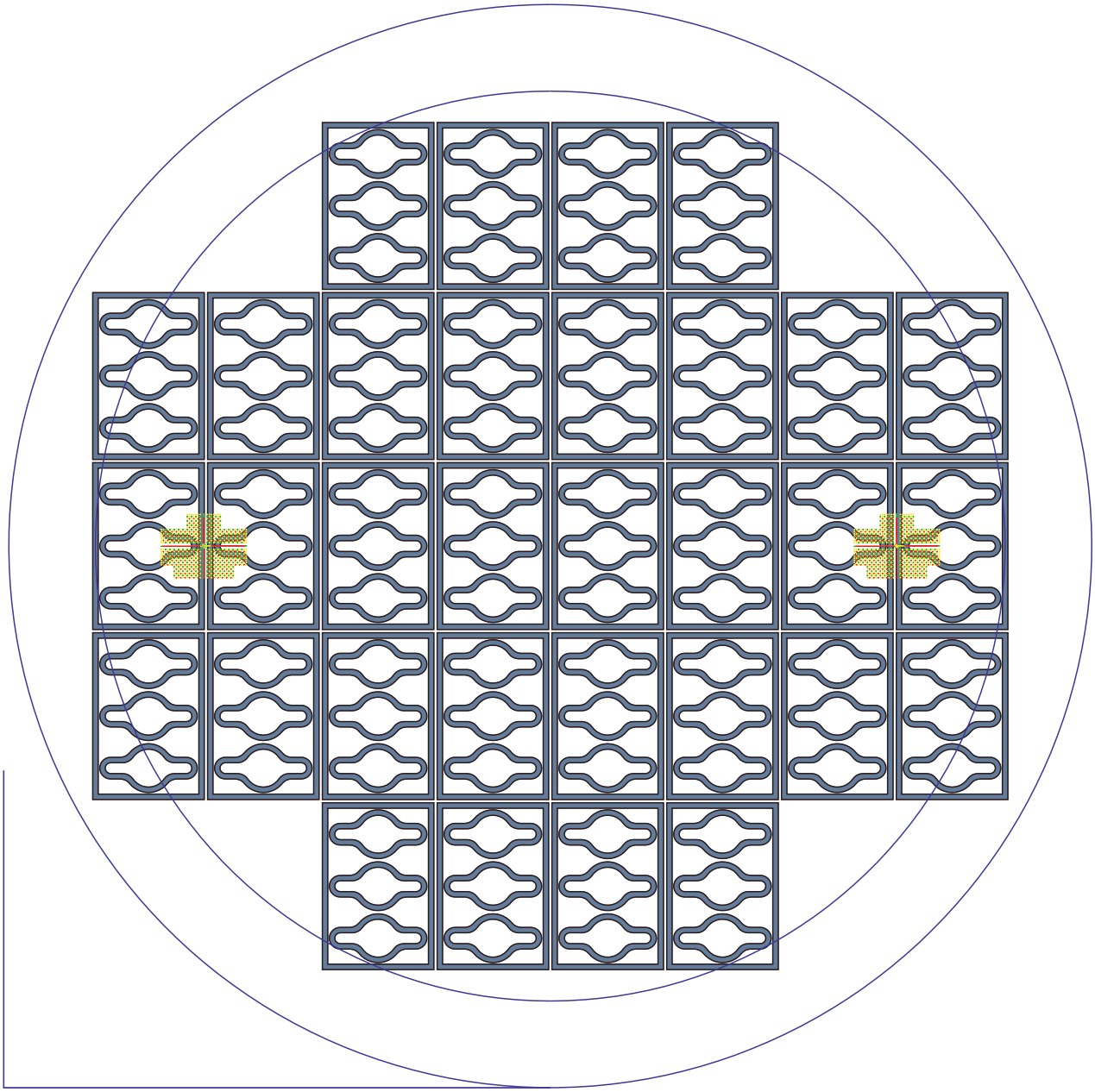

Figure B: Mask for Cu-layer structuring on the top wafer.

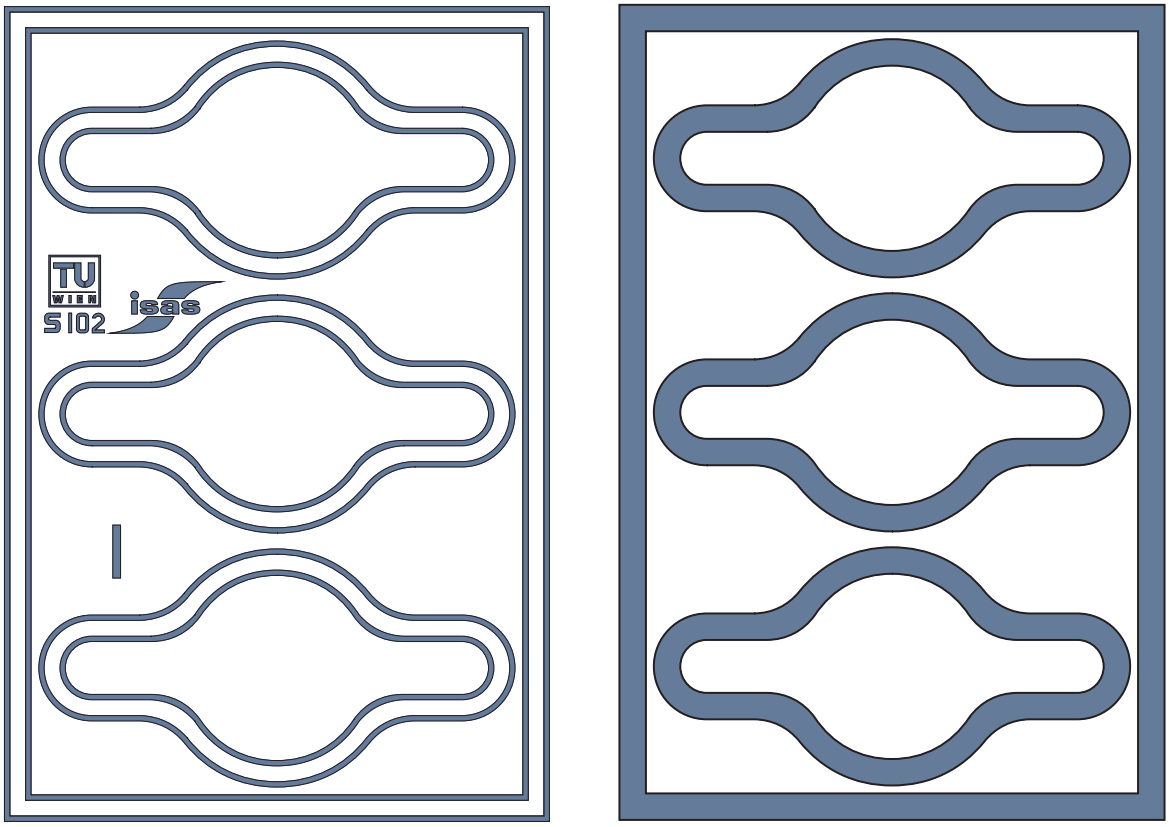

Figure C: Mask layouts for structuring of SU-8 (left) and Cu (right) for one chip.

Literature

[1] URL http://www.who.int/mediacentre/factsheets/fs297/en/index.html

[2] URL http://seer.cancer.gov/csr/1975_2006/

[3] Ruddon, R., *Cancer Biology*, Oxford University Press, 4th edition, **2007**, ISBN 0-1950-9691-6

[4] Tracqui, P., "Biophysical models of tumour growth", *Rep Prog Phys*, 72:1–30, **2009**, doi:doi:10.1088/0034-4885/72/5/056701

[5] Valentijn, A., Zouq, N., and Gilmore, A., "Anoikis", *Biochem Soc Trans*, 32:421–425, **2004**

[6] Patra, S. K., "Dissecting lipid raft facilitated cell signaling pathways in cancer", *Biochim Biophys Acta*, 1785:182–206, **2008**

[7] Douma, S., van Laar, T., Zevenhoven, J., Meuwissen, R., van Garderen, E., and Peeper, D. S., "Suppression of anoikis and induction of metastasis by the neurotrophic receptor TrkB", *Nature*, 430:1034–1040, **2004**

[8] Zwielly, A., Gopas, J., Brkic, G., and Mordechai, S., "Discrimination between drug-resistant and non-resistant human melanoma cell lines by FTIR spectroscopy", *Analyst*, 134:294–300, **2009**, doi:10.1039/b805223a

[9] URL http://www.sigmaaldrich.com/

[10] Stoler, M. H. and Schiffman, M., "Interobserver reproducibility of cervical cytologic and histologic interpretations: realistic estimates from the ASCUS-LSIL Triage Study", *JAMA*, 285:1500–1505, **2001**, doi:10.1001/jama.285.11.1500

[11] Kriege, M., Brekelmans, C. T. M., Peterse, H., Obdeijn, I. M., Boetes, C., Zonderland, H. M., Muller, S. H., Kok, T., Manoliu, R. A., Besnard, A. P. E., Tilanus-Linthorst, M. M. A., Seynaeve, C., Bartels, C. C. M., Meijer, S., Oosterwijk, J. C., Hoogerbrugge, N., Tollenaar, R. A. E. M., de Koning, H. J., Rutgers, E. J. T., and Klijn, J. G. M., "Tumor characteristics and detection method in the MRISC screening program for the early detection of hereditary breast cancer", *Breast Cancer Res Treat*, 102:357–363, **2007**, doi:10.1007/s10549-006-9341-6

[12] Kendall, C., Isabelle, M., Bazant-Hegemark, F., Hutchings, J., Orr, L., Babrah, J., Baker,

R., and Stone, N., "Vibrational spectroscopy: a clinical tool for cancer diagnostics", *Analyst*, 134:1029–1045, **2009**, doi:10.1039/b822130h

[13] van den Driesche, S., Witarski, W., Pastorekova, S., and Vellekoop, M. J., "A quadruple wavelength IR sensor system for label-free tumour screening", *Meas Sci Technol*, 20:124015, **2009**, doi:10.1088/0957-0233/20/12/124015

[14] van den Driesche, S., Witarski, W., and Vellekoop, M. J., "3.0-3.7 µm infrared sensor system for cell analysis", in: "Proceedings of SPIE vol. 7362", pp. 73620Y–73620Y–9, Dresden, Germany, **May 2009**, ISBN 9780819476364, doi:10.1117/12.822058

[15] van den Driesche, S., Witarski, W., and Vellekoop, M. J., "CH_2-symmetric/CH_2-antisymmetric stretch ratio sensor for cell analysis", in: O. Dössel and W. C. Schlegel, (Editors) "World Congress on Medical Physics and Biomedical Engineering, September 7 - 12, 2009, Munich, Germany", volume 25/VIII of *IFMBE Proceedings*, pp. 15–18, Springer, Munich, Germany, **Sept. 2009**, ISBN 978-3-642-03472-5

[16] van den Driesche, S., Witarski, W., Hafner, C., Kittler, H., and Vellekoop, M. J., "A mid infrared LED-photodiode based sensor for cell analysis", in: "Proc. IEEE Sensors", pp. 1562–1566, **October 25-28, 2009**, doi:10.1109/ICSENS.2009.5398482

[17] Stuart, B. H., *Infrared Spectroscopy - Fundamentals and Applications (Analytical Techniques in the Sciences (AnTs))*, Wiley, **2004**, ISBN 0764119257

[18] URL http://old.iupac.org/goldbook/A00035.pdf

[19] URL http://mivim.gel.ulaval.ca/dynamique/index.php?idD=58&Lang=1

[20] URL http://www.lsbu.ac.uk/water/vibrat.html

[21] Tamm, L. K. and Tatulian, S. A., "Infrared spectroscopy of proteins and peptides in lipid bilayers", *Q Rev Biophys*, 30:365–429, **1997**, doi:10.1017/S003358359700337

[22] Alberts, B., *Molecular Biology of the Cell*, New York: Garland Science, 5th edition, **2007**

[23] URL http://www.bioteach.ubc.ca/

[24] URL http://biology.clc.uc.edu/courses/bio104/lipids.htm

[25] Rigas, B., Morgello, S., Goldman, I. S., and Wong, P. T., "Human colorectal cancers display abnormal Fourier-transform infrared spectra", *Proc Natl Acad Sci U S A*, 87:8140–8144, **1990**

[26] Maziak, D. E., Do, M. T., Shamji, F. M., Sundaresan, S. R., Perkins, D. G., and Wong, P. T. T., "Fourier-transform infrared spectroscopic study of characteristic molecular structure in cancer cells of esophagus: an exploratory study", *Cancer Detect Prev*, 31:244–253, **2007**, doi:10.1016/j.cdp.2007.03.003

[27] Anastassopoulou, J., Boukaki, E., Conti, C., Ferraris, P., Giorgini, E., Rubini, C., Sabbatini, S., Theophanides, T., and Tosi, G., "Microimaging FT-IR spectroscopy on pathological breast tissues", *Vib Spectrosc*, 51:270–275, **2009**, doi:10.1016/j.vibspec.2009.07.005

[28] Fabian, H., Thi, N. A., Eiden, M., Lasch, P., Schmitt, J., and Naumann, D., "Diagnosing benign and malignant lesions in breast tissue sections by using IR-microspectroscopy", *Biochim Biophys Acta*, 1758:874–882, **2006**, doi:10.1016/j.bbamem.2006.05.015

[29] Piccart, M. J., Wood, W. C., Hung, C. M., Solin, J. L., and Cardoso, F., *Breast Cancer and Molecular Medicine*, Springer, **2006**, ISBN 3-540-28265-3

[30] Schulz, W. A., *Molecular Biology of Human Cancers (An Advanced Student's Text)*, Springer, **2005**, ISBN 1-4020-3185-8

[31] Felding-Habermann, B., "Integrin adhesion receptors in tumor metastasis", *Clinical and Experimental Metastasis*, 20:203–213, **2003**, doi:10.1023/A:1022983000355

[32] URL http://www.cta.tuwien.ac.at/cavs/equipment.php

[33] URL http://www.nir-spektroskopie.de/geraete/equinoxe.htm

[34] URL http://www.carlroth.nl/website/nl-nl/pdf/Zellpassage_Trypsin_E.pdf

[35] URL http://www.genengnews.com/transfection/ATCC_TechBulletin_7_Final_06_07.pdf

[36] URL www.invitrogen.com

[37] Venyaminov, S. Y. and Prendergast, F. G., "Water (H_2O and D_2O) Molar Absorptivity in the 1000-4000 cm^{-1} Range and Quantitative Infrared Spectroscopy of Aqueous Solutions", *Anal Biochem*, 248:234–245, **1997**, doi:10.1006/abio.1997.2136

[38] Kim, Y., Hankyu, N., and Chung, H., "Determination of the Equilibrium Constant of the Isotropic Disproportionation Between Water and Heavy Water Using Near-Infrared Spectroscopy", *Applied Spectroscopy*, 63(2):256–259, **2009**, doi:10.1366/000370209787391996

[39] Abgrall, P., Conedera, V., Camon, H., Gue, A.-M., and Nguyen, N.-T., "SU-8 as a structural material for labs-on-chips and microelectromechanical systems", *Electrophoresis*, 28:4539–4551, **2007**, doi:10.1002/elps.200700333

[40] Lorenz, H., Despont, M., Fahrni, N., LaBianc, N., Renaudy, P., and Vettigerx, P., "SU-8: a low-cost negative resist for MEMS", *J Micromech Microeng*, 7:121–124, **1997**, doi:10.1088/0960-1317/7/3/010

[41] URL www.korth.de

[42] Kulka, S., Kaun, N., Baena, J. R., Frank, J., Svasek, P., Moss, D., Vellekoop, M. J., and Lendl, B., "Mid-IR synchrotron radiation for molecular specific detection in microchip-based analysis systems", *Anal Bioanal Chem*, 378:1735–1740, **2004**, doi:10.1007/s00216-004-2534-0

[43] Hinsmann, P., Frank, J., Svasek, P., Harasek, M., and Lendl, B., "Design, simulation and application of a new micromixing device for time resolved infrared spectroscopy of chemical reactions in solution", *Lab Chip*, 1:16–21, **2001**, doi:10.1039/b104391a

[44] Kölhed, M., Hinsmann, P., Svasek, P., Frank, J., Karlberg, B., and Lendl, B., "On-line

fourier transform infrared detection in capillary electrophoresis", *Anal Chem*, 74:3843–3848, **2002**, doi:10.1021/ac025590t

[45] Svasek, P., Svasek, E., Lendl, B., and Vellekoop, M. J., "Fabrication of miniaturized fluidic devices using SU-8 based lithography and low temperature wafer bonding", *Sens Actuators A*, 115:591–599, **2004**, doi:10.1016/j.sna.2004.03.055